



CERN-EP-2022-256
17 November 2022

J/ψ production at midrapidity in p–Pb collisions at $\sqrt{s_{NN}} = 8.16$ TeV

ALICE Collaboration*

Abstract

The production of inclusive, prompt and non-prompt J/ψ was studied for the first time at midrapidity ($-1.37 < y_{\text{cms}} < 0.43$) in p–Pb collisions at $\sqrt{s_{NN}} = 8.16$ TeV with the ALICE detector at the LHC. The inclusive J/ψ mesons were reconstructed in the dielectron decay channel in the transverse momentum (p_T) interval $0 < p_T < 14$ GeV/ c and the prompt and non-prompt contributions were separated on a statistical basis for $p_T > 2$ GeV/ c . The study of the J/ψ mesons in the dielectron channel used for the first time in ALICE online single-electron triggers from the Transition Radiation Detector, providing a data sample corresponding to an integrated luminosity of $689 \pm 13 \mu\text{b}^{-1}$. The proton–proton reference cross section for inclusive J/ψ was obtained based on interpolations of measured data at different centre-of-mass energies and a universal function describing the p_T -differential J/ψ production cross sections. The p_T -differential nuclear modification factors R_{pPb} of inclusive, prompt, and non-prompt J/ψ are consistent with unity and described by theoretical models implementing only nuclear shadowing.

arXiv:2211.14153v2 [nucl-ex] 2 Oct 2023

*See Appendix A for the list of collaboration members

1 Introduction

Differential measurements of J/ψ mesons in heavy-ion collisions at the LHC give insight into their production mechanisms, pointing to a significant contribution from regeneration at low p_{T} , and give evidence for deconfinement in Pb–Pb collisions [1–6]. However, to better understand the underlying mechanisms and the influence of the quark–gluon plasma, reference measurements in proton–proton (pp) and proton–nucleus (p–A) collisions are crucial. Measurements in p–A collisions allow cold nuclear matter effects to be quantified. In p–Pb collisions at the LHC, parton shadowing or gluon saturation are considered to be the dominant effects influencing J/ψ production. These initial-state effects are expressed in terms of modified parton distribution functions in the nucleus (nPDF) or the color glass condensate effective theory [7–9]. Additional processes in the initial state, such as coherent parton energy loss, and final-state effects, where the $c\bar{c}$ states interact with the system generated in the small collision volume, have been predicted as well [10–13].

The inclusive J/ψ cross section includes contributions from prompt J/ψ , directly produced in the hadronic interaction or via feed-down from other directly produced charmonium states (e.g. χ_c and $\psi(2S)$), as well as non-prompt J/ψ originating from the decay of beauty hadrons. Thus, the influence of cold nuclear matter effects on open-heavy flavour production can be accessed as well through non-prompt J/ψ measurements ($b\text{-hadron} \rightarrow J/\psi + X$) in p–Pb collisions.

The ALICE, ATLAS, CMS and LHCb collaborations performed many differential measurements of J/ψ and open-beauty production at mid-, forward and backward rapidity in p–Pb collisions at $\sqrt{s_{\text{NN}}} = 5.02$ TeV [14–21] as well as at forward and backward rapidity at $\sqrt{s_{\text{NN}}} = 8.16$ TeV [22–24]. All the measurements can qualitatively be described by theoretical calculations including different combinations of the above-mentioned effects.

This article reports, for the first time, on the measurement of inclusive, prompt and non-prompt J/ψ mesons at midrapidity in p–Pb collisions at $\sqrt{s_{\text{NN}}} = 8.16$ TeV. At low p_{T} , the measurements reach Bjorken- x values of 10^{-4} to 10^{-3} . As the ALICE trigger strategy for p–Pb collisions at this energy only allocated a small portion of the bandwidth for minimum bias triggers, in order to maximise the live time for rare triggers, the presented studies were only possible thanks to the usage of single-electron triggers provided by the ALICE Transition Radiation Detector (TRD).

This article is organised as follows. A brief description of the ALICE detector with a focus on the detectors used for the analysis is given in Sec. 2, where the data sample and event selection are also discussed. The analysis details and the estimation of the systematic uncertainties are described in Sec. 3. To quantify possible modifications of the J/ψ production in p–Pb collisions, a reference p_{T} -differential cross section for pp collisions is obtained by interpolating measured data from different collision energies, as detailed in Sec. 4. The results are presented and discussed in Sec. 5. Finally, conclusions are drawn in Sec. 6.

2 Detector setup, data sample, and event selection

The ALICE detector [25, 26] is ideally suited to measure J/ψ production in the dielectron decay channel at midrapidity due to its low material budget as well as its excellent particle identification (PID) and transverse momentum resolution.

The global track reconstruction is performed using the Inner Tracking System (ITS) [27] as well as the Time Projection Chamber (TPC) [28], both covering the full azimuthal angle and pseudorapidity $|\eta| < 0.9$. The detectors are placed inside a solenoid magnet, providing a magnetic field of $B = 0.5$ T along the beam direction. The ITS includes 6 layers of silicon detectors (2 layers each of silicon pixel, drift, and strip detectors) and is used for the primary and secondary vertex reconstruction. The silicon pixel layers (SPD), which are the two innermost ones, are placed at radial distances of $r = 3.9$ and 7.6 cm from the nominal interaction point (IP). Tracks with hits in both SPD layers (only in the second layer)

have an impact parameter resolution better than $50 \mu\text{m}$ ($100 \mu\text{m}$) in the transverse plane for transverse momenta above $2 \text{ GeV}/c$, allowing the prompt and non-prompt J/ψ contributions to be separated on a statistical basis. The electron identification is based on the measurement of the specific ionisation energy loss (dE/dx) in the TPC, a cylindrical gaseous drift detector with dimensions $85 < r < 250$ cm along the radial and $|z| < 250$ cm along the beam direction from the IP.

To enrich samples of electrons and positrons at intermediate and high p_{T} , two online single-electron triggers¹ derived from information provided by the TRD [29] were deployed. The TRD consists of 522 chambers² arranged in 6 layers surrounding the TPC in full azimuth at a radial distance of 2.90 m to 3.68 m from the IP, and along the longitudinal direction in 5 stacks covering the pseudorapidity interval $|\eta| < 0.84$. Each chamber comprises a foam/fibre sandwich radiator, a drift volume and a multiwire proportional chamber filled with a Xe-CO₂ gas mixture. The measurement of the temporal evolution of the signal in the drift region allows track segments to be reconstructed in each chamber, as well as the specific ionisation energy loss of the charged particle and the transition radiation photons from electrons crossing the radiator with a Lorentz factor $\gamma > 800$ to be measured. Due to the fast readout and subsequent online reconstruction of the TRD signals, where a transverse momentum and an electron likelihood³ is calculated within a stack from the individual track segments, a trigger decision on individual tracks with p_{T} and likelihood thresholds is made about $6 \mu\text{s}$ after the collision (level-1 trigger decision).

Furthermore, two scintillator arrays (V0) [31] placed along the beam direction at $-3.7 < \eta < -1.7$ and $2.8 < \eta < 5.1$ are used for triggering and event characterisation.

The analysis discussed in this article is based on data recorded in 2016 during the LHC heavy-ion run, where lead ions and protons were collided at a centre-of-mass energy per nucleon pair of $\sqrt{s_{\text{NN}}} = 8.16$ TeV. Data were taken with two beam configurations, where the directions of the proton and lead beams were swapped. With respect to the laboratory frame, the proton–lead centre-of-mass frame is shifted by $\Delta y_{\text{NN}} = 0.465$ towards the incoming proton beam for both beam configurations, leading to a rapidity coverage of $-1.37 < y_{\text{cms}} < 0.43$. Minimum bias (MB) events (level-0) were selected based on the coincident signal of both V0 scintillator arrays. The trigger is fully efficient for recording events with inclusive J/ψ mesons. Only a small sample of MB events was recorded and used for the J/ψ analysis at low p_{T} and to evaluate the TRD trigger performance. The two single-electron triggers were run with p_{T} thresholds of 2 and 3 GeV/ c and two different thresholds of the electron (positron) likelihood. The different efficiencies for electrons and positrons arise from the $E \times B$ effect⁴ [29]. To reduce the background of electrons from photon conversions in the detector material, especially at large radii outside the TPC, 5 track segments per stack and a track segment in the first layer were required. In addition, a cut on the sagitta ($\Delta p_{\text{T}}^{-1} < 0.2 \text{ c}/\text{GeV}$) was applied. These trigger selection criteria result in a reduction of the geometrical acceptance, because, due to individual inactive chambers, about 20% of the stacks do not contribute to the trigger decision [29].

Figure 1 shows, as an example the acceptance times efficiency (ϵ_{TRD}) of the TRD trigger with the online p_{T} threshold at 2 GeV/ c for electrons (left) and positrons (right) considering all trigger selection criteria. The trigger turn-on curve results were obtained in the offline analysis as a function of the globally re-

¹The TRD trigger selects online electrons and positrons. Throughout the article the term ‘electron trigger’ denotes both electron and positron.

²Eighteen chambers are not installed in front of the PHOTon Spectrometer [30] to reduce the material budget in front of this detector.

³The total accumulated charge of each track segment is translated into an electron likelihood via a transformation function, stored in the form of a one-dimensional look-up table in the front-end electronics of the detector. The electron likelihood of a track is then obtained as the average of the likelihood values of the associated track segments.

⁴In the chambers, the direction of the drift electric field is perpendicular to that of the magnetic field, which affects the direction of the drifting electrons such that it is approximately aligned with the negative tracks and systematically rotated relative to the positive tracks. This leads to differences in performance of the track segment reconstruction and the electron likelihood calculation.

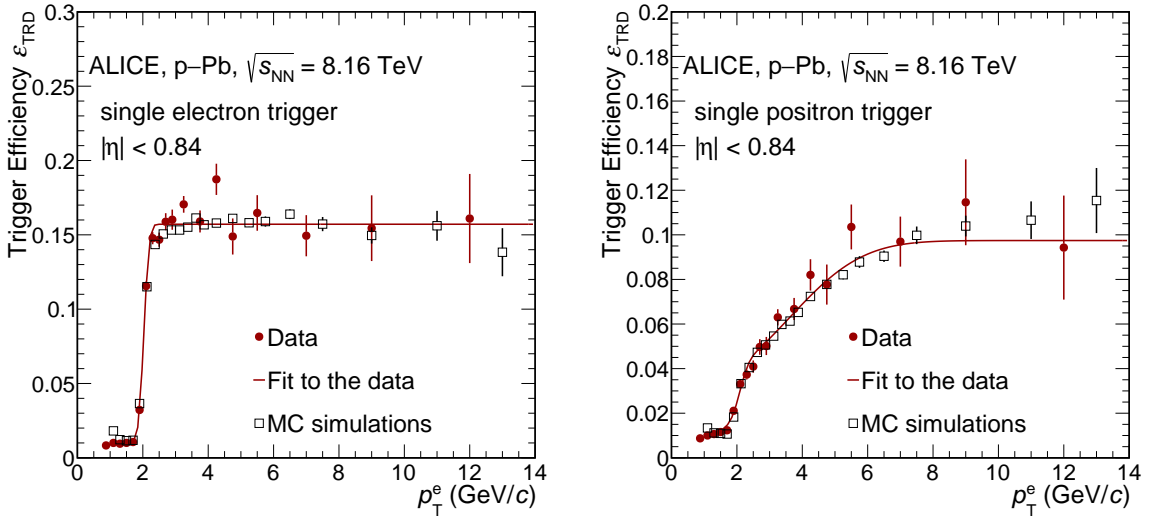


Figure 1: Acceptance times efficiency of the TRD trigger with the p_T threshold at 2 GeV/c for single electrons (left) and single positrons (right) obtained from data and MC simulations. See text for details.

constructed p_T by identifying electrons and positrons using the TPC in MB data (N_e^{MB}) and the fraction of these that satisfy the online TRD trigger decisions ($N_e^{MB,TRD}$): $\varepsilon_{TRD}(p_T) = \frac{N_e^{MB,TRD}(p_T)}{N_e^{MB}(p_T)}$. The TRD trigger efficiency shows small variations as a function of time, as the gain of the gas detector depends on pressure and gas composition affecting both the electron and positron efficiencies. In addition, the downscaling factor of the MB trigger was modified during the data taking period. Thus, to compute the correct efficiencies for the measurement, the single-electron trigger efficiencies determined in MB data were studied as a function of time and weighted by the number of TRD-triggered events in each time interval. The p_T threshold is clearly visible as a sharp rise at 2 GeV/c, followed by a constant plateau at an efficiency value determined by the geometrical and the electron identification selection criteria outlined above. The entries at low p_T are either electrons or positrons in events that were recorded because a high- p_T electron or positron in the same event satisfied the online trigger condition. The difference in the trigger turn-on curves for electrons and positrons is due to the $E \times B$ effect and it is well reproduced in Monte Carlo (MC) simulations (see next section). To guide the eye, the turn-on curve of electrons is fitted by an error function with an offset to describe the underlying event. For positrons, another error function is added to better describe the slower rise of the distribution.

Events selected by either of the two single-electron triggers are considered for further analysis, and to ensure a uniform detector acceptance, only events with a primary vertex located within 10 cm from the IP along the beam direction are accepted. Beam–gas interactions and pile-up events were rejected offline using information from the V0 and SPD detectors, together with algorithms identifying more than one vertex within an event, as described in Ref. [26]. The remaining fraction of pile-up events is negligible. These selection criteria result in MB and TRD-triggered data samples of about 50 million and 10 million events, corresponding to an integrated luminosity of $24.2 \pm 0.5 \mu\text{b}^{-1}$ and $689 \pm 13 \mu\text{b}^{-1}$, respectively.

3 Data analysis

The measurements of inclusive, prompt, and non-prompt J/ψ production were performed in a similar way to previous analyses in pp and p–Pb collisions at other centre-of-mass energies [20, 32–34]. However, in this article TRD-triggered events were used for the first time for the J/ψ analysis. The minimum J/ψ p_T of the TRD-triggered analysis is 2 GeV/c, where the single-electron efficiencies result in a J/ψ efficiency of about 10% increasing with rising p_T , as shown in Sec. 3.1. For the measurement in the p_T interval

0–2 GeV/c, the small available MB data sample was used.

In a first step, tracks with good quality were selected, which in addition had to fulfil the requirement of a minimum transverse momentum of 1 GeV/c and a pseudorapidity of $|\eta| < 0.84$ to reject tracks outside the TRD kinematic acceptance. For the inclusive analysis, to reduce the background originating from photon conversions at larger radii, tracks were required to have a hit in the first SPD layer. Also, in order to further suppress this contamination in the inclusive analysis, electrons (positrons) paired with positrons (electrons) in the same event yielding an invariant mass below $0.05 \text{ GeV}/c^2$ were rejected. The requirements on the SPD layers for the separation of the prompt and non-prompt J/ψ are outlined in Sec. 3.2.

The electron and positron identification is based on the measurement of the specific ionisation energy loss in the TPC. The selection criterion is n_{σ_e} , which is defined as the difference between the measured and expected signal in units of the detector resolution, for a specific particle hypothesis (i). Particles satisfying the condition $|n_{\sigma_e}| < 3.0$ were thus identified as electrons. Pions and protons were rejected by excluding tracks that were compatible within $3 n_{\sigma_{\pi,p}}$ with the corresponding particle hypothesis. For tracks with momenta $p > 5 \text{ GeV}/c$, the rejection criterion was reduced to $2 n_{\sigma_{\pi,p}}$ to increase the J/ψ reconstruction efficiency at high p_T . For the MB analysis, the selection criterion for electrons and positrons was set to $-2 < n_{\sigma_e} < 3$ to improve the signal-to-background ratio at low p_T .

The efficiencies of the applied selection criteria and of the TRD trigger were obtained from MC simulations. The EPOS-LHC model [35] was used to simulate minimum bias p–Pb collisions, into which one J/ψ meson per event was embedded. The prompt J/ψ mesons were generated with a flat rapidity distribution and a realistic p_T distribution taken from the J/ψ measurement in the dimuon decay channel at forward rapidity at the same centre-of-mass energy [23]. For the non-prompt J/ψ , PYTHIA 6.4 [36] was used to generate the $b\bar{b}$ pairs hadronising into beauty hadrons, subsequently forced to decay into J/ψ . The J/ψ decays were then simulated using the EvtGen package [37] together with the PHOTOS model [38] for a proper description of the QED radiative decay channel ($J/\psi \rightarrow e^+e^-\gamma$). The MC simulation assumes the prompt J/ψ to be unpolarised, while the non-prompt J/ψ have a small residual polarisation arising from the contributions of the different b-hadron decay channels as implemented in EvtGen [37]. All generated particles were transported through the ALICE detector setup using a GEANT3 model [39] considering a realistic detector response and reproducing the detector performance during the data taking. The TRD trigger was emulated in the simulation, i.e. the same selection criteria were calculated and applied as in real data.

3.1 Inclusive J/ψ analysis

The number of raw J/ψ candidates was extracted in p_T intervals from the invariant mass distribution (m_{ee}) of electron–positron pairs after background subtraction. Figure 2 shows the invariant mass distribution before background subtraction for two illustrative p_T intervals. The background is composed of pairs of electrons and positrons with different physics origin (uncorrelated background) and to a small extent, of electrons from common sources such as $c\bar{c}$ and $b\bar{b}$ decays or jet fragmentation (correlated background). Both background sources, see Fig. 2, are estimated by means of a hybrid method using the mixed-event technique (ME) for the uncorrelated background and a fitting function for the residual background, as applied in the analyses of minimum bias pp collisions at $\sqrt{s} = 5$ and 13 TeV [32, 33]. The mixed-event background distribution was normalised in the mass interval $2 < m_{ee} < 4 \text{ GeV}/c^2$ to the measured distribution of the same-event like-sign pairs, as these are expected to be little affected by correlated sources. After subtraction of the ME background, the residual distribution was then fitted with a polynomial of second order and a MC template for the J/ψ signal. Counting the number of electron–positron pairs in the mass interval $2.92 < m_{ee} < 3.16 \text{ GeV}/c^2$, after subtracting all background sources, yields the raw number of J/ψ candidates.

The p_T -differential cross section was obtained by correcting the number of J/ψ candidates found in a

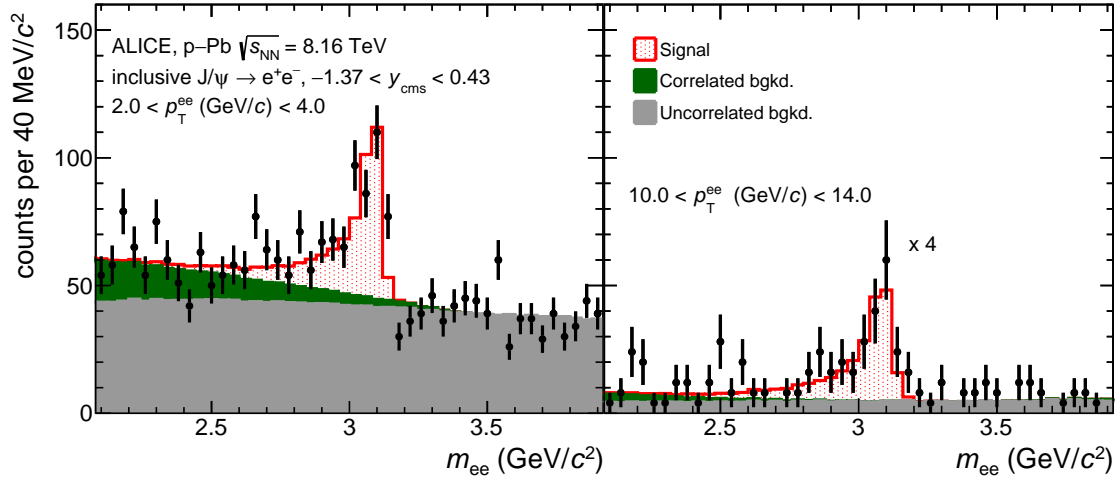


Figure 2: Invariant mass distribution of e^+e^- pairs from J/ψ decays and from correlated and uncorrelated background sources for the lowest (left) and the highest (right) p_T interval considered in the analysis. For the highest p_T interval, the distributions were scaled by a factor 4 for better visibility.

given transverse momentum (Δp_T) and rapidity (Δy) interval by the average acceptance and efficiency ($\langle Acc \times \epsilon_{reco} \times \epsilon_{mass} \times \epsilon_{TRDtrg} \rangle$) in these intervals:

$$\frac{d\sigma^2}{dydp_T} = \frac{N_{J/\psi}^{raw}}{\langle Acc \times \epsilon_{reco} \times \epsilon_{mass} \times \epsilon_{TRDtrg} \rangle \times BR \times \Delta y \Delta p_T \times \mathcal{L}_{int}}, \quad (1)$$

where BR denotes the branching ratio of J/ψ to dielectrons ($5.97 \pm 0.03\%$) [40]. The integrated luminosity of the data sample is given by $\mathcal{L}_{int} = \frac{N_{MB}}{\sigma_{MB}}$, where σ_{MB} is the MB trigger cross section obtained from van der Meer scans [41]. The number of MB events $N_{MB} = N_{TRD} \times f_{norm}$ was calculated from the number of TRD-triggered events N_{TRD} and the normalisation factor f_{norm} . The latter corresponds to the inverse probability of an MB event being triggered by the TRD as well. Its statistical uncertainty amounts to 0.35%. The evaluation of f_{norm} was cross-checked with an alternative method based on the online counters, provided by the central trigger processor, of the number of inspected events at level-0 (MB) and level-1 (TRD-triggered). The ratio of the two numbers is corrected for the slightly different efficiency in event selection in both data samples. Due to the larger number of level-0 trigger counts, this ratio has a smaller statistical uncertainty and agrees on the few per-mill level with the result from the first method. Thus the statistical uncertainty of the first described method is used as the systematic uncertainty of the normalisation factor f_{norm} . For the MB analysis, neither the TRD trigger efficiency nor the trigger normalisation factor f_{norm} apply.

The acceptance and efficiency factors, determined via the aforementioned MC simulations, correct for the kinematic acceptance (Acc), the reconstruction efficiency and the applied selection criteria (ϵ_{reco}), the TRD trigger efficiency for J/ψ mesons (ϵ_{TRDtrg}) and the mass interval chosen to count the J/ψ signal candidates (ϵ_{mass}). The individual contributions and the total efficiency are shown in Fig. 3 (left). The TRD trigger algorithm was emulated in the simulation. The same quantities such as electron likelihood, online p_T , and number of track segments per stack as in real data were calculated and the analogous trigger decision was derived. By comparing the distributions of these quantities for electrons and positrons in data and MC simulations, it was ensured that the TRD trigger is correctly implemented in simulation and shows the same performance as in data. Figure 3 (right) shows as an example the excellent agreement of the electron and positron likelihood in data and MC simulations for the single-electron trigger with a p_T threshold at 2 GeV/c.

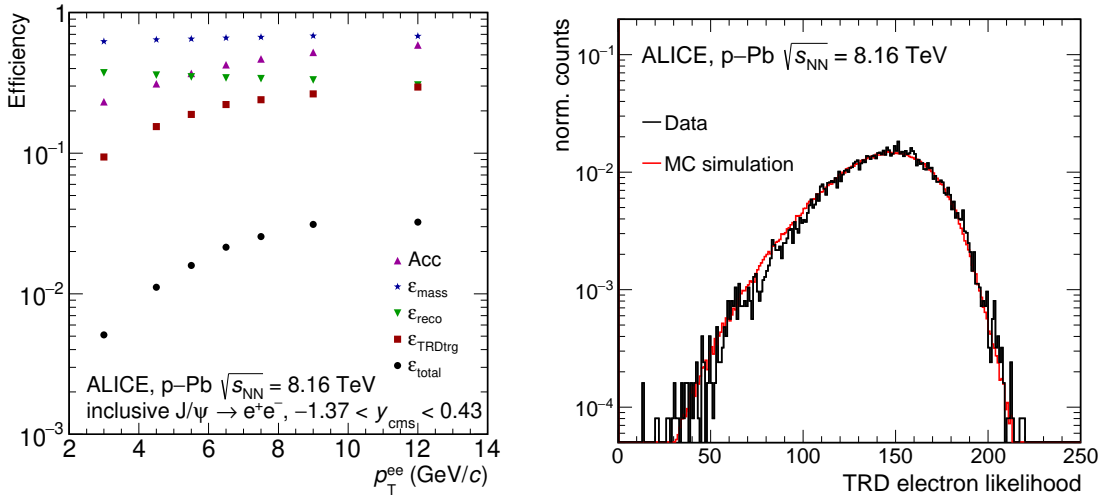


Figure 3: (Left) Efficiency as a function of transverse momentum for the inclusive J/ψ analysis of the TRD-triggered data. (Right) Electron likelihood estimated from TRD for electrons identified using the TPC particle identification capabilities in data and MC simulations. The electron likelihood is stored in hardware as an unsigned 8-bit value (translating into integer values from 0 to 255).

The following sources of systematic uncertainties were considered for the determination of the inclusive J/ψ cross section: (i) track reconstruction efficiency, (ii) electron identification, (iii) signal extraction, (iv) kinematics of the J/ψ used in the MC simulation, and (v) TRD trigger efficiency (does not apply to the analysis of the MB data sample). The uncertainty of the track reconstruction efficiency is related to the ITS–TPC matching efficiency and to the track selection criteria. No statistically significant systematic effects were found when rerunning the analysis with variations of the track selection criteria, with the exception of the requirement of the number of hits in the SPD layers (hit in first or both layers of the SPD). To estimate the influence of the SPD criterion, a data-driven technique, where pions tagged as belonging to identified K_S^0 decay topologies were used to determine the single-track uncertainty. The latter was then propagated to the two-track level (J/ψ) using a phase space simulation of the J/ψ decay to dielectrons. This uncertainty was found to amount to 3.1%, independent of the pair p_T . It was verified using MC simulations that the single-track uncertainty obtained with pions is identical to the one of electrons. Likewise, the uncertainty of the ITS–TPC matching efficiency, describing the probability that a track reconstructed in the TPC also has matching hits in the ITS, was estimated in a data-driven procedure as described in [42] and found to be independent of particle species. The uncertainty was propagated to the two track level (J/ψ) and amounts to 2%, independent of p_T . The two uncertainties were added in quadrature and are considered to be correlated across p_T intervals.

The uncertainty due to the particle identification was determined using electrons from photon conversions, pions from K_S^0 and protons from Λ decays, topologically reconstructed in data and MC simulations. The comparisons of the electron identification efficiency and hadron rejection in data and MC simulations under variations of the PID selection criteria yield a 2% p_T -independent uncertainty for the J/ψ meson. The uncertainty is considered correlated across p_T intervals.

The raw J/ψ yield was corrected for the average acceptance and efficiency in a given p_T interval and is thus sensitive to the kinematic distribution of the inclusive J/ψ mesons used in the MC simulation. To estimate the related uncertainty, the p_T spectrum of J/ψ mesons in the same rapidity range in p–Pb at $\sqrt{s_{NN}} = 5.02$ TeV [20] was fitted with a power law; then, new distributions were derived by varying the obtained parameters according to the correlation matrix provided by the fit procedure. For each iteration the average acceptance and efficiency in the given p_T interval was recomputed and the RMS of all values with respect to the default value was taken as uncertainty. In most of the p_T intervals the uncertainty is

negligible; the largest value, 0.2%, is found in the lowest p_T interval.

The signal extraction uncertainty is composed of contributions from the background description and the J/ψ signal distribution. The uncertainty related to the background description was determined by choosing different fitting functions for the correlated and uncorrelated background. The studies were performed in two p_T intervals (2–6 and 6–14 GeV/ c) with similar background distributions to avoid the statistical uncertainties dominating the systematic uncertainties. The variations show a deviation with respect to the default value of 1.9% for both p_T intervals. The uncertainty associated with the J/ψ signal shape was found by varying the mass interval used to count the raw J/ψ candidates. To reduce statistical fluctuations, the root mean square of all values with respect to the central value was determined for the p_T -integrated case resulting in an uncertainty of 1.3%.

The uncertainty of the TRD trigger efficiency was estimated based on MC simulations, where the threshold of the electron and positron likelihood value for the trigger decision was varied by an amount corresponding to the granularity with which it is calculated in the front-end electronics, and then the trigger efficiency for J/ψ mesons was recalculated. The resulting uncertainty is 2.3%. The adopted threshold variation is larger than the one expected from the observed changes in pressure and gas composition, that would lead to a change in gain and thus a change in the electron efficiency of the trigger.

The systematic uncertainties of all sources described above were added in quadrature and amount to a total systematic uncertainty of 5.2% for all p_T intervals. The total systematic uncertainty of the MB analysis is 4.7%. The branching ratio uncertainty, the MB trigger cross section uncertainty (including also a contribution from its stability over time, as discussed in Ref. [41]), and the uncertainty of the TRD trigger normalisation factor f_{norm} are added in quadrature to obtain a global normalisation uncertainty of 2%. As the latter contribution is small, this uncertainty also holds for the MB analysis.

3.2 Determination of the non-prompt J/ψ fraction

The non-prompt J/ψ fraction (f_b) was determined as in previous analyses [20, 34, 43–45] on a statistical basis. The method relies on the property that J/ψ mesons originating from b-hadron decays have, in the studied kinematic range, a decay vertex distribution extending to values well beyond the secondary vertex resolution, in contrast to prompt J/ψ . As a very good pointing resolution is needed, only J/ψ candidates with at least one of the decay products having hits in both SPD layers were accepted.

The measurement of the fraction f_b was carried out via a minimisation of a two-dimensional unbinned negative log-likelihood fit in p_T intervals, where the invariant mass and the pseudoproper decay length (x) distributions of the electron-positron pairs were simultaneously fitted:

$$-\ln L = -\sum_{i=1}^N \ln F(x, m_{ee}). \quad (2)$$

The variable N denotes the number of J/ψ candidates in the invariant mass interval $2.4 < m_{ee} < 3.6$ GeV/ c^2 and $F(x, m_{ee})$ is given as

$$F(x, m_{ee}) = f_{\text{sig}} \times F_{\text{sig}}(x) \times M_{\text{sig}}(m_{ee}) + (1 - f_{\text{sig}}) \times F_{\text{bkgd}}(x) \times M_{\text{bkgd}}(m_{ee}), \quad (3)$$

where f_{sig} is the fraction of e^+e^- pairs attributed to prompt and non-prompt J/ψ within the invariant mass interval $2.4 < m_{ee} < 3.6$ GeV/ c^2 . $M_{\text{sig}}(m_{ee})$ and $F_{\text{sig}}(x)$ are the functional forms describing the invariant mass and pseudoproper decay length distributions of the signal. $M_{\text{bkgd}}(m_{ee})$ and $F_{\text{bkgd}}(x)$ are the corresponding functional forms of the background component. The pseudoproper decay length is defined as $x = \frac{c \times L_{xy} \times m_{J/\psi}}{p_T}$, where L_{xy} is the transverse projection of the vector from the primary vertex of the event to the J/ψ decay vertex and $m_{J/\psi}$ is the J/ψ pole mass [40]. The signal is composed of a prompt and non-prompt J/ψ contribution

$$F_{\text{sig}}(x) = f_b^{\text{raw}} \times F_b(x) + (1 - f_b^{\text{raw}}) \times F_p(x), \quad (4)$$

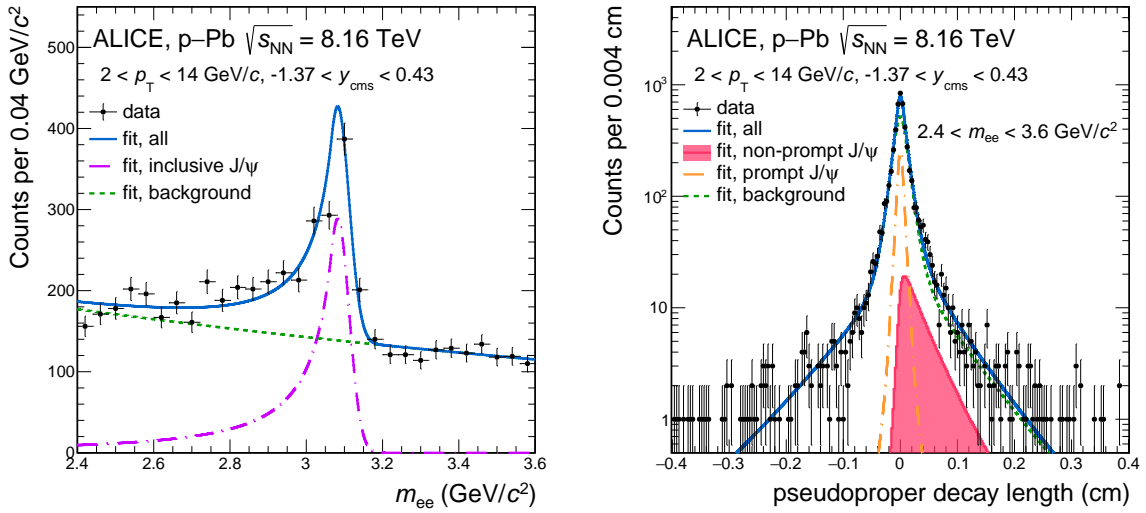


Figure 4: Invariant mass (left) and pseudoproper decay length (right) distributions for e^+e^- pairs in the p_T interval $2 < p_T < 14$ GeV/c. Only statistical uncertainties are shown. The one-dimensional projections of the different contributions of the fit as described in the text are drawn for each distribution.

where f_b^{raw} is the uncorrected fraction of non-prompt J/ψ and $F_b(x)$ and $F_p(x)$ are the pseudoproper decay length distributions of non-prompt and prompt J/ψ , respectively.

The invariant mass and pseudoproper decay length distributions of e^+e^- pairs are shown as an example for the p_T interval $2 < p_T < 14$ GeV/c in Fig. 4. The one-dimensional projections of the different components of the fit are drawn for each distribution. The invariant mass distribution is described in the fit by a Crystal Ball function [46] and an exponential function for the signal and background contributions, respectively. The parameters of the Crystal Ball function were tuned to match the J/ψ signal shape in MC, which describes well the measured invariant mass distribution of inclusive J/ψ mesons presented in this article. The analysis of the non-prompt J/ψ fraction was carried out for $p_T > 2$ GeV/c in coarser momentum intervals than the inclusive analysis to reduce statistical fluctuations.

The pseudoproper decay length distribution of prompt J/ψ , known as the resolution function $R(x)$, is given by the finite detector resolution and reconstruction algorithm. The resolution function was determined from MC simulations and is well described by the sum of two Gaussian distributions at its core, with the addition of a power law function for the tails, symmetric around $x = 0$. To minimise discrepancies in the $R(x)$ description between data and MC simulations, the distance-of-closest-approach (DCA) to the primary vertex in the transverse plane for single tracks was tuned in MC simulations via a data-driven approach. In this approach, differences in the mean and width of the DCA distributions were corrected for in MC simulations as a function of p_T , azimuthal angle and SPD hit configuration, which strongly influences the DCA resolution, using primary pions to match the performance in data. The RMS of the resolution function shows, as expected, a strong dependence on the J/ψ p_T with values of about $156 \mu\text{m}$ ($43 \mu\text{m}$) for a J/ψ p_T of 2 GeV/c (12 GeV/c). The pseudoproper decay length distribution of non-prompt J/ψ is modelled by the kinematic distribution of J/ψ from b-hadron decays obtained from the MC simulation convoluted with the resolution function. The relative fractions of the different b-hadron species were reweighted in the MC simulations to match the measurements performed by the LHCb collaboration in pp collisions at $\sqrt{s} = 13$ TeV [47]. These measurements are consistent with the results, available in a coarser p_T binning, by the LHCb collaboration in p–Pb collisions at $\sqrt{s_{\text{NN}}} = 8.16$ TeV [24]. As the background contribution changes with invariant mass, see Fig. 4 (left), $F_{\text{bkgd}}(x)$ was obtained by fitting the pseudoproper decay length distributions from the side bands of the invariant mass distribution ($2.4 < m_{ee} < 2.8$ GeV/c² and $3.2 < m_{ee} < 3.6$ GeV/c²) and interpolating the background contribution

Table 1: Systematic uncertainties (in percent) of the p_{T} -differential and p_{T} -integrated f_{b} measurements.

Sources	p_{T} (GeV/c)					
	2–4	4–6	6–8	8–10	10–14	2–14
MC input p_{T} shape	3.0	1.6	1.0	0.8	0.5	6.7
Resolution function $R(x)$	3.4	1.0	0.5	0.4	0.4	1.3
x distr. of non-prompt J/ψ ($F_{\text{b}}(x)$)	6.4	1.1	1.7	2.2	0.5	3.8
x distr. of bkgd ($F_{\text{bkgd}}(x)$)	3.3	3.7	2.0	1.6	2.1	3.8
Inv. mass p.d.f. of signal ($M_{\text{sig}}(m_{\text{ee}})$)	2.6	1.9	0.6	2.2	4.8	2.1
Inv. mass p.d.f. of bkgd ($M_{\text{bkgd}}(m_{\text{ee}})$)	1.5	0.6	0.1	2.4	0.1	0.6
Total	9.0	4.7	2.9	4.3	5.3	9.0

under the J/ψ signal peak ($2.8 < m_{\text{ee}} < 3.2$ GeV/ c^2) assuming a linear combination of the background in the left and right side band. The relative fraction of each contribution was included as an additional free parameter in the global fitting.

The final f_{b} was then obtained by correcting $f_{\text{b}}^{\text{raw}}$ by the average acceptance and efficiency of prompt ($\langle A \times \varepsilon \rangle_{\text{P}}$) and non-prompt ($\langle A \times \varepsilon \rangle_{\text{b}}$) J/ψ in a given p_{T} interval:

$$f_{\text{b}} = \left(1 + \frac{1 - f_{\text{b}}^{\text{raw}}}{f_{\text{b}}^{\text{raw}}} \times \frac{\langle A \times \varepsilon \rangle_{\text{b}}}{\langle A \times \varepsilon \rangle_{\text{P}}} \right)^{-1}. \quad (5)$$

The factors $\langle A \times \varepsilon \rangle$ obtained from the MC simulations are slightly different for prompt and non-prompt J/ψ due to the different p_{T} distributions. For a more realistic treatment, the p_{T} distributions in the MC simulations were reweighted to match measurements of prompt and non-prompt J/ψ mesons performed by the LHCb collaboration at forward rapidity in p–Pb collisions at $\sqrt{s_{\text{NN}}} = 8.16$ TeV [22].

The systematic uncertainties of the f_{b} measurement arising from the imprecise knowledge of the probability distributions used in the two-dimensional fit as well as from the input MC p_{T} distributions of prompt and non-prompt J/ψ affecting the $\langle A \times \varepsilon \rangle$ correction factors are summarised in Table 1.

To estimate the systematic uncertainty related to the calculation of the average correction factors ($\langle A \times \varepsilon \rangle$), the p_{T} distributions in MC were not reweighted with the measurements by the LHCb collaboration, but instead with ALICE measurements at midrapidity in p–Pb collisions at $\sqrt{s_{\text{NN}}} = 5.02$ TeV [20]. Due to the coarse binning and the large uncertainties, the central values of the ALICE measurement were fitted with a power law function, which was then used in the reweighting procedure. The differences in the f_{b} fractions corrected with the $\langle A \times \varepsilon \rangle$ factors obtained from different p_{T} shapes were then taken as systematic uncertainties. The uncertainties are largest for the p_{T} -integrated case as well as at low p_{T} , where the p_{T} distributions rapidly change. As in previous analyses, possible systematic uncertainties due to polarisation are not considered as the measured degree of polarisation is small in pp collisions [48–50] and no measurement yet exists for p–Pb collisions. In the MC simulations used, no polarisation is implemented for prompt J/ψ, while due to the contributions of the different b-hadron species a small polarisation arises for non-prompt J/ψ as implemented in EvtGen. Assuming no polarisation also for non-prompt J/ψ would lead, as studied in Ref. [20], to a 4% (1%) variation of $\langle A \times \varepsilon \rangle$ at low (high) p_{T} .

The description of the DCA distribution for single tracks in the MC simulation was improved via a data-driven approach using charged pions to reduce the systematic uncertainties of the resolution function $R(x)$. To study the influence of bremsstrahlung for electrons, the DCA resolution was varied based on the observed resolution difference between electrons and pions in the MC simulation. Two extreme scenarios were considered: one where the bremsstrahlung effect is twice as large in data as in MC, and the other where the bremsstrahlung effect is null in data. The f_{b} values were extracted for both hypotheses and the differences with respect to the standard scenario were taken as the systematic uncertainty of the resolution function $R(x)$.

The p_T -differential spectra of the b-hadron species used as input for building the pseudoproper decay length distribution $F_b(x)$ of e^+e^- pairs from non-prompt J/ψ decays were simulated using PYTHIA 6.4 [36], which yields compatible results to those obtained with FONLL [51–53]. As the latter describes measurements in the b-hadron sector in pp collisions well [43, 54, 55], no additional systematic uncertainties related to the p_T -shapes were added. Uncertainties related to the decay kinematics were studied using PYTHIA 6.4 instead of the event generator EvtGen and the absolute differences in the resulting f_b values were assigned as the systematic uncertainties of the functional forms of the pseudoproper decay length of non-prompt J/ψ.

The $F_{\text{bkgd}}(x)$ uncertainties were evaluated by changing the width of the side band regions as well as the extrapolated region under the signal peak.

The systematic uncertainties related to the signal and background templates used for fitting the invariant mass distributions of the e^+e^- pairs were estimated by exchanging the MC J/ψ signal shape with one including only pairs originating from radiative or non-radiative decays, and by using different background fit functions (first and second order polynomials) as well as the invariant mass distribution of the same-sign electron pairs. The usage of the MC signal shape with either only radiative or non-radiative decays leads to extreme variations of the tail of the invariant mass distribution towards lower masses. The differences between the f_b values resulting from the aforementioned variations of the template and the default f_b values were taken as a systematic uncertainty.

Studies with a dedicated MC simulation showed that differences in TRD trigger efficiency for prompt and non-prompt J/ψ are negligible.

All the aforementioned uncertainties were added in quadrature yielding the total uncertainties listed in Table 1.

4 Proton–proton reference

In order to evaluate the impact of nuclear effects on the inclusive as well as prompt and non-prompt J/ψ production in p–Pb collisions, reference cross sections are needed which reflect the production in the absence of cold nuclear matter and hot-medium related effects. Since measurements in proton-proton collisions at the same collision energy are not available, the reference distributions had to be obtained from measured data at different centre-of-mass energies. The procedures are described in the following.

4.1 Reference for the inclusive J/ψ analysis

The calculation of the inclusive J/ψ production cross section at $\sqrt{s} = 8.16$ TeV is based on an assumption on the shape of the J/ψ p_T -differential cross section as well as an interpolation between measured results at different collision energies to obtain the p_T -integrated cross section and the average transverse momentum ($\langle p_T \rangle$). With a suitable transformation, the J/ψ p_T -differential cross section can be described by a universal function [56], independent of collision energy and rapidity. The universal function is defined as

$$\frac{\langle p_T \rangle}{d\sigma/dy} \times \frac{d^2\sigma}{dydp_T} = \frac{2(n-1) \cdot C^2 \times p_T / \langle p_T \rangle}{(1 + C^2 \times (p_T / \langle p_T \rangle)^2)^n}, \quad (6)$$

with $C = \Gamma(3/2)\Gamma(n-3/2)/\Gamma(n-1)$, where n is left as the only free fit parameter if the values of the p_T -integrated J/ψ cross section and $\langle p_T \rangle$ are known. The universal function was fitted to the available J/ψ data [18, 32, 49, 57–62], which range from 1.96 to 13 TeV in centre-of-mass energy with a p_T range from zero to 20 GeV/c, resulting in $n = 3.45 \pm 0.05$. The uncertainty of the parameter n was obtained by excluding individual J/ψ measurements and repeating the fit. Once the $\langle p_T \rangle$ and the p_T -integrated cross section are known, the p_T -differential reference at $\sqrt{s} = 8.16$ TeV can then be calculated.

The $\langle p_T \rangle$ value of 2.86 ± 0.03 GeV/c at $\sqrt{s} = 8.16$ TeV was evaluated from the fit function $\langle p_T \rangle(\sqrt{s}) = a + b \times \log(\sqrt{s})$, which describes the evolution of the measured $\langle p_T \rangle$ at midrapidity well over three orders of magnitude as a function of collision energy from 0.2 to 13 TeV [33].

For the interpolation of the p_T -integrated J/ψ cross section at midrapidity, it is assumed that the collision-energy dependence of J/ψ production is the same as the one of $c\bar{c}$ quark pair production. As FONLL describes the available measurements of $\sigma_{c\bar{c}}$ well [63], the p_T -integrated J/ψ production cross section was estimated by scaling the $c\bar{c}$ cross sections calculated by FONLL with the PDF set CTEQ 6.6 [51–53]. The $c\bar{c}$ cross section $\sigma_{c\bar{c}}(|y| < 0.5) = d\sigma_{c\bar{c}}/dy$ was calculated for midrapidity and for $p_T < 50$ GeV/c for all collision energies from 0.2 to 13 TeV for which measurements of the p_T -integrated J/ψ production cross section at midrapidity and low p_T exist [32, 33, 57, 64–66]. Via a χ^2 minimisation, the collision energy dependence of the FONLL cross sections was scaled to the measured J/ψ production cross sections showing a good agreement between the energy dependence of the FONLL calculations and the one of the measured data. The model uncertainties, i.e. the charm quark mass, renormalisation and factorisation scales, are large, but were assumed to be fully correlated over the collision energy and thus should not change the shape of the energy dependence. The cross section was then extracted by evaluating the scaled FONLL curve at $\sqrt{s} = 8.16$ TeV. For the estimation of the statistical and systematic uncertainties of the scaling procedure, each data point was shifted by its statistical or systematic uncertainty, respectively, independently from the other data points, i.e. the uncertainties were assumed to be uncorrelated across collision energies. These variations were repeated multiple times leading to a Gaussian distribution with the mean being the evaluated central J/ψ cross section value and the width providing a 1σ uncertainty. The resulting p_T -integrated J/ψ cross section at $\sqrt{s} = 8.16$ TeV and midrapidity ($|y| < 0.9$) is $\text{BR} \times \frac{d\sigma}{dy} = 452.3 \pm 2.1$ (stat.) ± 16.5 (syst.) nb.

Using the universal function and the parameters obtained above, the p_T -differential J/ψ production cross section was calculated for the same p_T intervals as the p–Pb measurement. The resulting pp reference is shown in Fig. 5 (left) scaled by the Pb mass number ($A = 208$). The systematic uncertainty has a correlated and uncorrelated component across p_T intervals. The correlated uncertainty originates from the interpolated p_T -integrated J/ψ cross section and is about 3.8%. The uncorrelated uncertainty is composed of the statistical and systematic uncertainty of the input p_T spectra and $\langle p_T \rangle$ as well as the shape uncertainty of the universal fit function. The latter is the dominating contribution to the uncertainty and was estimated to be 1% for $p_T < 7$ GeV/c and 5% above. It was determined by comparing the p_T shape obtained with the universal fit function to the measured distributions for several collision energies. For illustration purposes, the correlated and uncorrelated uncertainties were added in quadrature and are shown as a grey band in Fig. 5 (left).

4.2 Reference for the non-prompt J/ψ fraction analysis

The non-prompt J/ψ fraction f_b as a function of p_T in pp collisions shows a slight dependence on centre-of-mass energy. As no measured pp reference at $\sqrt{s} = 8.16$ TeV exists, the p_T -differential f_b fractions were obtained via an interpolation method based on measurements available at midrapidity at other centre-of-mass energies ranging from 1.96 TeV to 13 TeV [18, 34, 57, 58, 67]. At each energy with available measurements, the p_T -differential f_b values with their statistical and systematic uncertainties added in quadrature were fitted with a function. The latter was obtained as the ratio of the FONLL calculated p_T -differential production cross section of non-prompt J/ψ and the universal function representing the inclusive J/ψ measurement (see Sec. 4.1). The parameters of the universal fit function were not constrained, to allow for the varying p_T -dependence of f_b measured at each collision energy. For the fit results at each energy a 1σ uncertainty band was obtained based on the experimental uncertainties of the considered measurements as well as the FONLL uncertainties (beauty quark mass, renormalisation and factorisation scale), with the latter being the dominant contribution.

In the next step, the f_b fractions evaluated in narrow p_T intervals from the fitted functions were parameterised as a function of centre-of-mass energy assuming a linear dependence to obtain the f_b value for $\sqrt{s} = 8.16$ TeV. Repeating this procedure with the upper and lower edge of the 1σ uncertainty band of the fit function yielded the systematic uncertainties of the f_b values used as pp reference. Replacing the linear function by a power law or exponential function resulted in a negligible systematic uncertainty.

As the p_{T} intervals used in this analysis are coarse and the f_{b} values change within the p_{T} intervals, the average f_{b} values and their related uncertainties were then determined for each p_{T} interval using the p_{T} distribution as a weight. The uncertainty amounts to 6% in the first p_{T} interval, $2 < p_{\text{T}} < 4$ GeV/c, and is negligible above.

5 Results

The p_{T} -differential production cross section of inclusive J/ψ in p–Pb collisions at $\sqrt{s_{\text{NN}}} = 8.16$ TeV is shown in Fig. 5 (left). The statistical and systematic uncertainties are shown as bars and boxes, respectively. The measurements cover the p_{T} intervals 0–2 GeV/c and from 2 up to 14 GeV/c obtained from the MB and the TRD-triggered data samples, respectively. The usage of the single-electron triggers provided by the TRD strongly enhances the number of J/ψ measured at intermediate and high p_{T} .

As expected for the higher collision energy, the p_{T} -differential production cross section at $\sqrt{s_{\text{NN}}} = 8.16$ TeV is consistently above the measurement at $\sqrt{s_{\text{NN}}} = 5.02$ TeV, albeit the shapes are very similar for $p_{\text{T}} > 2$ GeV/c. Also depicted in Fig. 5 (left) is the pp reference spectrum for $\sqrt{s} = 8.16$ TeV obtained as discussed in Sec. 4 and scaled by the mass number of Pb ($A = 208$). It can be observed that the modifications in p–Pb compared to pp collisions are small for $p_{\text{T}} > 2$ GeV/c.

To quantify the nuclear effects, the nuclear modification factor R_{pPb} is calculated from the production cross sections in p–Pb and pp collisions:

$$R_{\text{pPb}} = \frac{d^2 \sigma_{\text{J}/\psi}^{\text{pPb}} / dy dp_{\text{T}}}{A \times d^2 \sigma_{\text{J}/\psi}^{\text{pp}} / dy dp_{\text{T}}}, \quad (7)$$

where A is the mass number of the Pb nucleus and $d^2 \sigma_{\text{J}/\psi}^{\text{pPb}} / dy dp_{\text{T}}$ and $d^2 \sigma_{\text{J}/\psi}^{\text{pp}} / dy dp_{\text{T}}$ are the p_{T} -differential production cross sections in p–Pb and pp collisions at the same collision energy. The nuclear modification factor is expected to be equal to unity in the absence of nuclear effects.

Figure 5 (right) shows the p_{T} -differential R_{pPb} values for inclusive J/ψ production. The error bars represent the statistical uncertainties, the boxes the systematic uncertainties. The latter were derived by adding in quadrature the systematic uncertainties of the p–Pb result and the systematic uncertainties correlated in p_{T} of the pp reference spectrum. The uncorrelated uncertainties of the pp reference spectrum are shown as a band around unity. The normalisation uncertainty is shown as a box around unity at zero p_{T} .

For $p_{\text{T}} > 2$ GeV/c, the R_{pPb} is consistent with unity. This tendency was already observed at the lower energy of $\sqrt{s_{\text{NN}}} = 5.02$ TeV. The data indicate that nuclear effects do not exceed 20% in the kinematic range above $p_{\text{T}} = 2$ GeV/c taking into account the deviation from unity and the related statistical and systematic uncertainties. The R_{pPb} for $p_{\text{T}} < 2$ GeV/c from the MB analysis is, considering uncertainties, larger than the one at the lower centre-of-mass energy by two standard deviations. However, no significant conclusion can be drawn due to the limited size of the MB data sample.

To enhance the precision of the p_{T} -integrated R_{pPb} value, an extrapolation down to zero- p_{T} of the cross section measured with the TRD-triggered data sample is used instead of the minimum bias result. The measured visible cross section for $p_{\text{T}} > 2$ GeV/c corresponds to about two-thirds of the p_{T} -integrated cross section at midrapidity. The extrapolation method uses the p_{T} -differential measurement in p–Pb collisions at $\sqrt{s_{\text{NN}}} = 5.02$ TeV assuming that cold nuclear matter effects influencing J/ψ production are the same at both collision energies. This is very well supported by the findings at forward and backward rapidity by the ALICE and LHCb collaborations within their present measurement accuracy [22, 23]. The extrapolation factor F was computed as the ratio of the cross section in the p_{T} interval 0–2 GeV/c to the one in 2–14 GeV/c. Taking into account the hardening of the p_{T} spectrum as observed in pp collisions between the two collision energies as estimated using the universal function (see Sec. 4) with the mean p_{T} parameters for each energy, the extrapolation factor $F = 0.46 \pm 0.04(\text{stat.}) \pm 0.04(\text{syst.})$

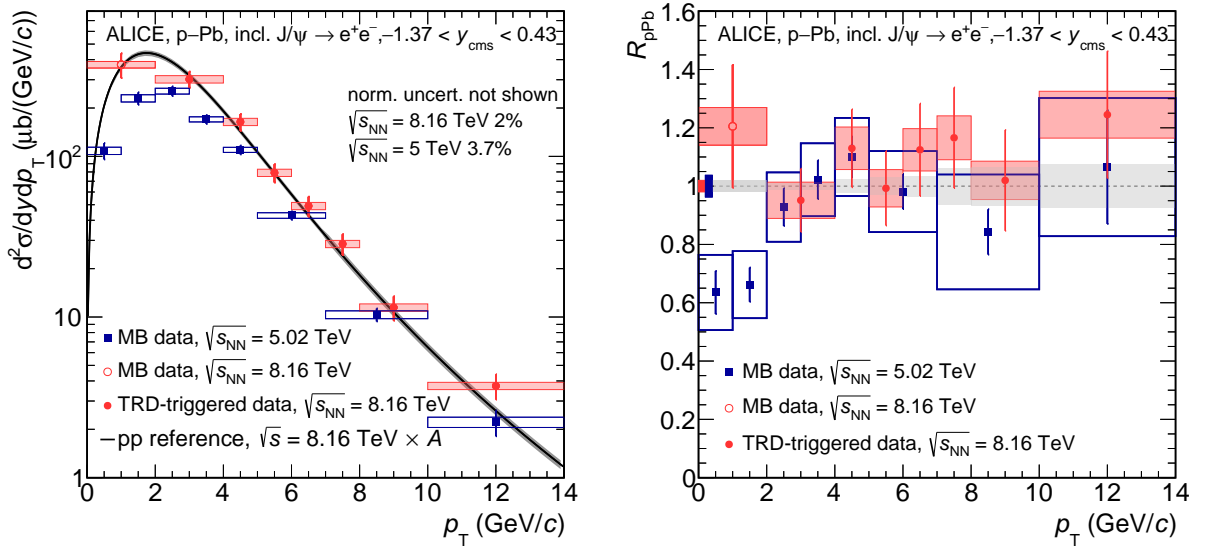


Figure 5: (left) p_T -differential inclusive J/ψ production cross section in MB and TRD-triggered p–Pb collisions at $\sqrt{s_{NN}} = 8.16$ TeV in comparison with the measurements at $\sqrt{s_{NN}} = 5.02$ TeV [20]. The statistical and systematic uncertainties are shown as error bars and boxes. Also depicted is the pp reference spectrum at $\sqrt{s} = 8.16$ TeV obtained via the procedure described in Sec. 4 and multiplied by the mass number of the Pb nucleus ($A = 208$). The grey band represents the combined correlated and uncorrelated uncertainties. (right) R_{pPb} of inclusive J/ψ in MB and TRD-triggered p–Pb collisions at $\sqrt{s_{NN}} = 5.02$ TeV and 8.16 TeV. The statistical and systematic uncertainties are shown as error bars and boxes. For the 8.16 TeV measurement, the uncorrelated uncertainties of the pp reference are shown as a band around unity. The normalisation uncertainties are shown as coloured boxes around unity at zero p_T .

was derived. The statistical and systematic uncertainties of the extrapolation factor were determined by adding in quadrature or linearly, respectively, the uncertainties of each p_T interval of the p–Pb 5.02 TeV cross section measurement. The systematic uncertainty also includes the uncertainties related to the evaluation of the hardening of the p_T spectrum and to possible differences in cold nuclear matter effects at both energies. The first contribution was determined by modifying the parameters of the universal function by the uncertainties of the mean p_T values for both energies, resulting in a modification of the F factor by 3%. The second contribution was estimated by computing the difference in the J/ψ cross section calculations including cold nuclear matter effects via the EPPS16 nPDF sets by Lansberg *et al.* [68, 69] at both energies, assuming the uncertainties of the calculations to be highly correlated between energies. Repeating the calculation of the F factor with the obtained difference yields a 2.5% uncertainty. All contributions to the total systematic uncertainty of the extrapolation factor F were added quadratically.

The extrapolated p_T -integrated inclusive J/ψ cross section is then given by:

$$\frac{d\sigma_{\text{inclusive } J/\psi}^{\text{extra}}}{dy} = (1 + F) \times \frac{d\sigma_{\text{inclusive } J/\psi}^{\text{vis}}}{dy} = 1409 \pm 89(\text{stat.}) \pm 84(\text{syst.}) \mu\text{b}, \quad (8)$$

where $\frac{d\sigma_{\text{inclusive } J/\psi}^{\text{vis}}}{dy} = 968 \pm 56(\text{stat.}) \pm 50(\text{syst.}) \mu\text{b}$ denotes the measured visible cross section of inclusive J/ψ in the p_T interval $2 < p_T < 14$ GeV/c at midrapidity ($-1.37 < y_{\text{cms}} < 0.43$) in p–Pb collisions at $\sqrt{s_{NN}} = 8.16$ TeV. The p_T -integrated R_{pPb} value, depicted in Fig. 6, was then obtained as in Eq. 7. The p_T -integrated cross section for pp collisions at the same collision energy was obtained via the interpolation method discussed in Sec. 4. The systematic uncertainties of the R_{pPb} value were calculated by adding in quadrature the systematic uncertainties of the extrapolated p_T -integrated inclusive J/ψ cross

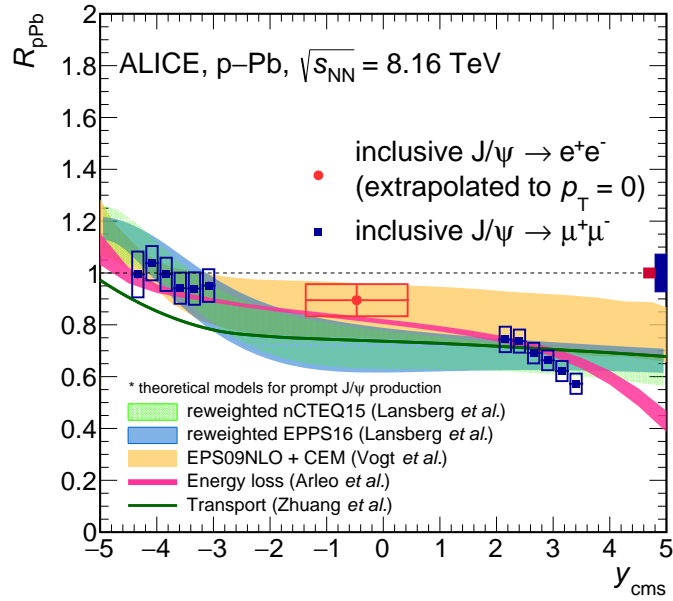


Figure 6: p_T -integrated R_{pPb} values for inclusive J/ψ production as a function of y_{cms} in comparison with results at forward and backward rapidity by the ALICE collaboration [23]. The statistical and systematic uncertainties are shown as error bars and boxes. The overall normalisation uncertainties are shown as boxes around unity at large y_{cms} . Also shown are the results of theoretical calculations which refer to prompt J/ψ [10, 12, 68, 73–76].

section in p–Pb and of the cross section in pp collisions.

Also shown in Fig. 6 are the ALICE measurements for inclusive J/ψ in the dimuon decay channel at forward ($2.03 < y_{cms} < 3.53$) and backward ($-4.46 < y_{cms} < -2.96$) rapidity [23] at the same collision energy, as well as several theoretical calculations for prompt J/ψ . The calculations by Lansberg *et al.* are based on the framework of NRQCD factorisation with nCTEQ15 and EPPS16 nPDF sets that were reweighted to include results from the RHIC and LHC colliders [68–70]. The calculation by Vogt *et al.* is based on a pure shadowing scenario employing the next-to-leading order (NLO) Color Evaporation Model (CEM) with the EPS09 shadowing parametrisation [71]. This older parton distribution function was obtained before collider data were available. The calculation by Arleo *et al.* [72] includes effects of momentum broadening, coherent parton energy loss and no nuclear shadowing of the gluon PDF. The model by Zhuang *et al.* [12] includes final-state effects (so-called hot nuclear matter effects), where the $c\bar{c}$ states interact with the system generated in the collision, as well as nuclear shadowing using the EPS09 gluon nPDF. The theoretical models describing the forward and backward rapidity results, also agree within uncertainties with the measurement at midrapidity. While the p_T -integrated inclusive yield is strongly dominated by the prompt J/ψ , the p_T -differential results for prompt and non-prompt J/ψ are separately compared with models, in the following part of this section.

The fraction of J/ψ originating from b -hadron decays (f_b) is shown as a function of J/ψ p_T in Fig. 7. In addition to the results presented in this article, similar measurements from p–Pb collisions at $\sqrt{s_{NN}} = 5.02$ TeV and from pp collisions at 7 and 8 TeV, performed by the ALICE and ATLAS collaborations, are depicted. For all data shown, the statistical and systematic uncertainties were added quadratically. The measurements show the complementarity of the experiments at the LHC; in particular ALICE provides measurements at low and intermediate p_T while ATLAS has results at high p_T . In the common p_T interval the results from the different experiments are in good agreement. The emerging picture is a rise of f_b with increasing p_T from values close to 0.1 in the 1–2 GeV/c interval to values exceeding 0.5 at p_T larger than 20 GeV/c. With the current experimental uncertainties, one cannot discern

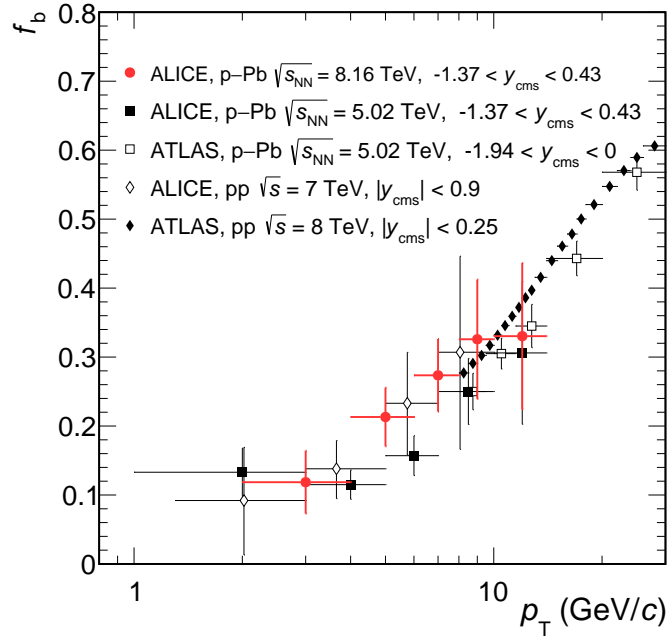


Figure 7: Fraction of J/ψ originating from b -hadron decays as a function of J/ψ p_T in comparison with analogous measurements, also at midrapidity, in pp and p–Pb collisions by the ALICE and ATLAS collaborations [20, 43, 67, 79]. The statistical and systematic uncertainties of the measurements were added in quadrature.

differences between the results for pp and p–Pb collisions or at different collision energies. The experimental precision at low and intermediate p_T is expected to significantly improve with the much larger data samples and tracking precision of the upgraded ALICE detector in LHC Runs 3 and 4 [77, 78].

The p_T -integrated fraction of non-prompt J/ψ for the p_T interval $2 < p_T < 14$ GeV/ c at midrapidity ($-1.37 < y_{cms} < 0.43$) in p–Pb collisions at $\sqrt{s_{NN}} = 8.16$ TeV is $f_b^{vis} = 0.18 \pm 0.03(\text{stat.}) \pm 0.02(\text{syst.})$. Using the integrated inclusive cross section in the same kinematic region, the prompt and non-prompt J/ψ cross sections per unit of rapidity were obtained as:

$$\begin{aligned} \frac{d\sigma_{\text{prompt } J/\psi}^{\text{vis}}}{dy} &= (1 - f_b^{\text{vis}}) \times \frac{d\sigma_{\text{inclusive } J/\psi}^{\text{vis}}}{dy} = 797 \pm 66(\text{stat.}) \pm 32(\text{syst.}) \mu\text{b} \quad \text{and} \\ \frac{d\sigma_{\text{non-prompt } J/\psi}^{\text{vis}}}{dy} &= f_b^{\text{vis}} \times \frac{d\sigma_{\text{inclusive } J/\psi}^{\text{vis}}}{dy} = 169 \pm 30(\text{stat.}) \pm 17(\text{syst.}) \mu\text{b}. \end{aligned} \quad (9)$$

The p_T -differential production cross sections of prompt and non-prompt J/ψ are displayed in the left- and right-hand panels of Fig. 8 together with the corresponding measurements at forward and backward rapidity released by the LHCb collaboration at the same centre-of-mass energy, and with the ALICE measurements at midrapidity at $\sqrt{s_{NN}} = 5.02$ TeV.

The cross section is larger at midrapidity compared to the corresponding measurements at forward and backward rapidity at the same centre-of-mass energy and shows a similar p_T dependence as the measurement at $\sqrt{s_{NN}} = 5.02$ TeV for $p_T > 2$ GeV/ c . The measurements are very well described by the calculations from P. Duwentäster *et al.* which utilise the latest version of the CTEQ15 nPDF set, the nCTEQ15HQ set [80]. Here, for the cross section calculations, the effective scattering matrix elements were determined from measurements in pp collisions in a data-driven approach following Ref. [81] and validated with NLO calculations in NRQCD for quarkonium and the general-mass variable-flavour-number scheme [82] for the open heavy-flavour mesons. To obtain this nPDF set, measurements from

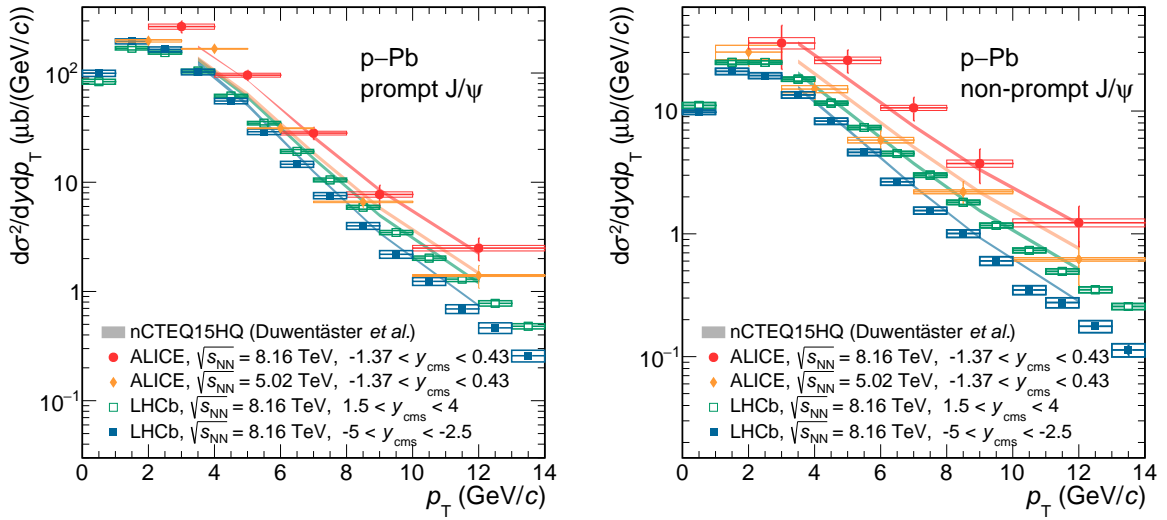


Figure 8: p_T -differential production cross sections of prompt (left) and non-prompt (right) J/ψ together with corresponding results at forward and backward rapidity by the LHCb collaboration [22] and ALICE measurements at midrapidity at $\sqrt{s_{NN}} = 5.02$ TeV [20]. The statistical and systematic uncertainties are represented as error bars and boxes for each data point. The normalisation uncertainties are not shown. The measurements are compared with calculations using the latest version of the CTEQ nPDFs, nCTEQ15HQ [80], see text for details.

the LHC on heavy quark and quarkonium production were used to constrain the gluon density down to Bjorken- $x \sim 10^{-5}$. Compared to the nCTEQ15 fit, not taking into account the LHC data, the uncertainty of the gluon PDF in Pb is reduced by a factor 3 around Bjorken- $x = 10^{-4}$. The measured prompt J/ψ spectrum at midrapidity is mostly driven by the nuclear gluon PDF in the Bjorken- x range 2×10^{-4} to 10^{-3} , where the ratio of the nuclear relative to the proton gluon PDF is 0.69–0.79 in the new nCTEQ15HQ fit.

The prompt and non-prompt J/ψ nuclear modification factors were calculated as

$$R_{pPb}^{\text{prompt } J/\psi} = \frac{1 - f_b^{\text{pPb}}}{1 - f_b^{\text{pp}}} \times R_{pPb} \quad \text{and} \quad (10)$$

$$R_{pPb}^{\text{non-prompt } J/\psi} = \frac{f_b^{\text{pPb}}}{f_b^{\text{pp}}} \times R_{pPb},$$

where R_{pPb} denotes the inclusive J/ψ nuclear modification factors shown in Fig. 5. The fractions of J/ψ originating from b -hadron decays in p–Pb and pp collisions are represented by f_b^{pPb} and f_b^{pp} , with the latter obtained via an interpolation procedure as discussed in Sec. 4.2.

The resulting nuclear modification factors are shown as a function of J/ψ p_T in Fig. 9 for $p_T > 2$ GeV/ c . The displayed systematic uncertainties, shown as open boxes, include the uncertainties of the f_b values for pp and p–Pb collisions as well as the correlated and uncorrelated uncertainties of the inclusive J/ψ R_{pPb} values. The prompt and non-prompt J/ψ nuclear modification factors are consistent with unity within statistical and systematic uncertainties. Measurements performed at midrapidity in p–Pb collisions at $\sqrt{s_{NN}} = 5.02$ TeV by the ALICE, ATLAS and CMS collaborations, shown for comparison, agree with our results for p_T above 2 GeV/ c , while the value for the lowest p_T bin for prompt J/ψ at $\sqrt{s_{NN}} = 5.02$ TeV from ALICE is significantly below unity.

Several theoretical calculations for prompt J/ψ , introduced before when discussing the rapidity dependence in Fig. 6, are shown for comparison with the measured p_T -differential R_{pPb} in Fig. 9 (left). Also

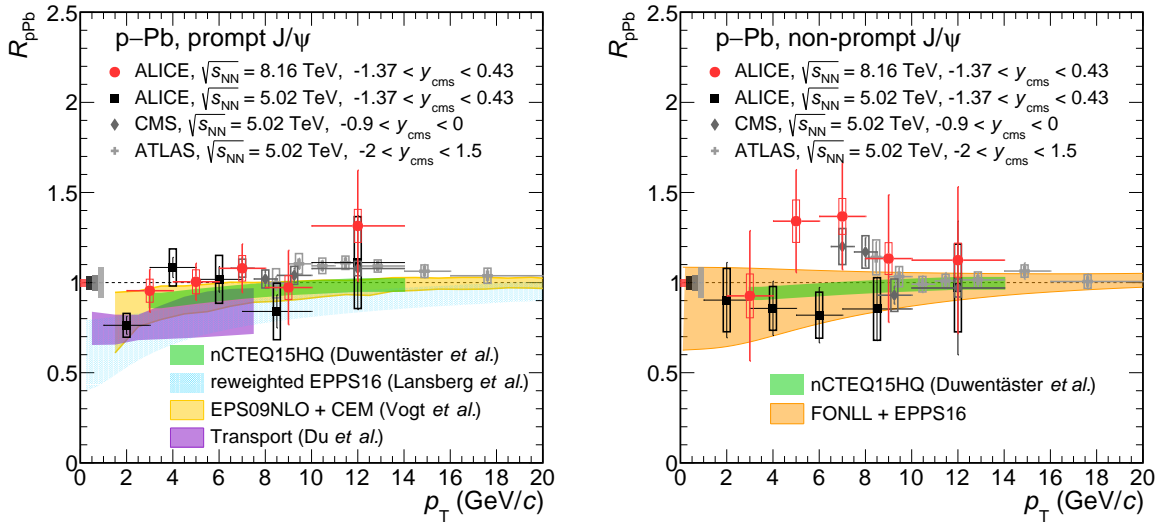


Figure 9: p_T -differential R_{pPb} of prompt (left) and non-prompt (right) J/ψ together with corresponding results in p–Pb collisions at $\sqrt{s_{NN}} = 5.02$ TeV [18, 20, 79] and theoretical calculations [13, 68, 74, 75, 80]. The statistical and systematic uncertainties are represented as error bars and boxes for each data point. The normalisation uncertainties are indicated as boxes around unity at zero p_T .

depicted is the transport calculation by Du *et al.* [13], based on the kinetic rate-equation approach within a fireball model and previously used for heavy-ion and d–Au collisions, for the p–Pb collision system. Shadowing effects were considered in the calculation by Vogt *et al.* via the pre-LHC EPS09 nPDFs. The theoretical calculations describe the low p_T data where the model should be applicable. The calculation by Lansberg *et al.* [68] tends to be systematically below the data in the p_T range below 10 GeV/c, only approaching unity at 20 GeV/c. The approach based on the CEM and EPS09 nPDFs as well as the NLO pQCD calculation of Duwentäser *et al.* are closest to the data. The latter calculation has the smallest uncertainties profiting from the latest version of the nCTEQ15HQ nPDF set. This is also the case for the corresponding studies on non-prompt J/ψ shown in Fig. 9 (right). Also shown are results from a FONLL computation employing EPPS16 nPDFs [75], whose uncertainties strongly increase with decreasing p_T .

6 Summary

This article presents for the first time the p_T -differential production cross sections and nuclear modification factors R_{pPb} of inclusive, prompt and non-prompt J/ψ at midrapidity ($-1.37 < y_{cms} < 0.43$) in p–Pb collisions at $\sqrt{s_{NN}} = 8.16$ TeV with the ALICE detector at the LHC. The measurements were made possible by the usage of online single-electron triggers provided by the Transition Radiation Detector. Within the experimental and theoretical model uncertainties, the p_T -differential cross sections are well described by the calculations assuming only nuclear modified PDFs, with no final-state effects. The consistency of the measured R_{pPb} value of prompt J/ψ with unity shows that in the studied kinematic range cold nuclear matter effects are modest, even smaller than predicted by most theoretical calculations.

Acknowledgements

The ALICE Collaboration would like to thank all its engineers and technicians for their invaluable contributions to the construction of the experiment and the CERN accelerator teams for the outstanding performance of the LHC complex. The ALICE Collaboration gratefully acknowledges the resources and support provided by all Grid centres and the Worldwide LHC Computing Grid (WLCG) collaboration. The ALICE Collaboration acknowledges the following funding agencies for their support in building

and running the ALICE detector: A. I. Alikhanyan National Science Laboratory (Yerevan Physics Institute) Foundation (ANSL), State Committee of Science and World Federation of Scientists (WFS), Armenia; Austrian Academy of Sciences, Austrian Science Fund (FWF): [M 2467-N36] and Nationalstiftung für Forschung, Technologie und Entwicklung, Austria; Ministry of Communications and High Technologies, National Nuclear Research Center, Azerbaijan; Conselho Nacional de Desenvolvimento Científico e Tecnológico (CNPq), Financiadora de Estudos e Projetos (Finep), Fundação de Amparo à Pesquisa do Estado de São Paulo (FAPESP) and Universidade Federal do Rio Grande do Sul (UFRGS), Brazil; Bulgarian Ministry of Education and Science, within the National Roadmap for Research Infrastructures 2020-2027 (object CERN), Bulgaria; Ministry of Education of China (MOEC), Ministry of Science & Technology of China (MSTC) and National Natural Science Foundation of China (NSFC), China; Ministry of Science and Education and Croatian Science Foundation, Croatia; Centro de Aplicaciones Tecnológicas y Desarrollo Nuclear (CEADEN), Cubaenergía, Cuba; Ministry of Education, Youth and Sports of the Czech Republic, Czech Republic; The Danish Council for Independent Research | Natural Sciences, the VILLUM FONDEN and Danish National Research Foundation (DNRF), Denmark; Helsinki Institute of Physics (HIP), Finland; Commissariat à l’Energie Atomique (CEA) and Institut National de Physique Nucléaire et de Physique des Particules (IN2P3) and Centre National de la Recherche Scientifique (CNRS), France; Bundesministerium für Bildung und Forschung (BMBF) and GSI Helmholtzzentrum für Schwerionenforschung GmbH, Germany; General Secretariat for Research and Technology, Ministry of Education, Research and Religions, Greece; National Research, Development and Innovation Office, Hungary; Department of Atomic Energy Government of India (DAE), Department of Science and Technology, Government of India (DST), University Grants Commission, Government of India (UGC) and Council of Scientific and Industrial Research (CSIR), India; National Research and Innovation Agency - BRIN, Indonesia; Istituto Nazionale di Fisica Nucleare (INFN), Italy; Japanese Ministry of Education, Culture, Sports, Science and Technology (MEXT) and Japan Society for the Promotion of Science (JSPS) KAKENHI, Japan; Consejo Nacional de Ciencia (CONACYT) y Tecnología, through Fondo de Cooperación Internacional en Ciencia y Tecnología (FONCICYT) and Dirección General de Asuntos del Personal Académico (DGAPA), Mexico; Nederlandse Organisatie voor Wetenschappelijk Onderzoek (NWO), Netherlands; The Research Council of Norway, Norway; Commission on Science and Technology for Sustainable Development in the South (COMSATS), Pakistan; Pontificia Universidad Católica del Perú, Peru; Ministry of Education and Science, National Science Centre and WUT ID-UB, Poland; Korea Institute of Science and Technology Information and National Research Foundation of Korea (NRF), Republic of Korea; Ministry of Education and Scientific Research, Institute of Atomic Physics, Ministry of Research and Innovation and Institute of Atomic Physics and University Politehnica of Bucharest, Romania; Ministry of Education, Science, Research and Sport of the Slovak Republic, Slovakia; National Research Foundation of South Africa, South Africa; Swedish Research Council (VR) and Knut & Alice Wallenberg Foundation (KAW), Sweden; European Organization for Nuclear Research, Switzerland; Suranaree University of Technology (SUT), National Science and Technology Development Agency (NSTDA), Thailand Science Research and Innovation (TSRI) and National Science, Research and Innovation Fund (NSRF), Thailand; Turkish Energy, Nuclear and Mineral Research Agency (TENMAK), Turkey; National Academy of Sciences of Ukraine, Ukraine; Science and Technology Facilities Council (STFC), United Kingdom; National Science Foundation of the United States of America (NSF) and United States Department of Energy, Office of Nuclear Physics (DOE NP), United States of America. In addition, individual groups or members have received support from: Marie Skłodowska Curie, European Research Council, Strong 2020 - Horizon 2020 (grant nos. 950692, 824093, 896850), European Union; Academy of Finland (Center of Excellence in Quark Matter) (grant nos. 346327, 346328), Finland; Programa de Apoyos para la Superación del Personal Académico, UNAM, Mexico.

References

- [1] ALICE Collaboration, S. Acharya *et al.*, “Centrality and transverse momentum dependence of inclusive J/ψ production at midrapidity in Pb–Pb collisions at $\sqrt{s_{NN}}=5.02$ TeV”, *Phys. Lett. B* **805** (2020) 135434, arXiv:1910.14404 [nucl-ex].
- [2] ALICE Collaboration, S. Acharya *et al.*, “Studies of J/ψ production at forward rapidity in Pb-Pb collisions at $\sqrt{s_{NN}} = 5.02$ TeV”, *JHEP* **02** (2020) 041, arXiv:1909.03158 [nucl-ex].
- [3] ALICE Collaboration, S. Acharya *et al.*, “J/ψ elliptic and triangular flow in Pb-Pb collisions at $\sqrt{s_{NN}} = 5.02$ TeV”, *JHEP* **10** (2020) 141, arXiv:2005.14518 [nucl-ex].
- [4] K. Zhou, N. Xu, Z. Xu, and P. Zhuang, “Medium effects on charmonium production at ultrarelativistic energies available at the CERN Large Hadron Collider”, *Phys. Rev. C* **89** (2014) 054911, arXiv:1401.5845 [nucl-th].
- [5] X. Du and R. Rapp, “Sequential Regeneration of Charmonia in Heavy-Ion Collisions”, *Nucl. Phys. A* **943** (2015) 147–158, arXiv:1504.00670 [hep-ph].
- [6] A. Andronic, P. Braun-Munzinger, M. K. Köhler, K. Redlich, and J. Stachel, “Transverse momentum distributions of charmonium states with the statistical hadronization model”, *Phys. Lett. B* **797** (2019) 134836, arXiv:1901.09200 [nucl-th].
- [7] J. P. Blaizot, F. Gelis, and R. Venugopalan, “High-energy pA collisions in the color glass condensate approach. 2. Quark production”, *Nucl. Phys. A* **743** (2004) 57–91, arXiv:hep-ph/0402257.
- [8] N. Armesto, “Nuclear shadowing”, *J. Phys. G* **32** (2006) R367–R394, arXiv:hep-ph/0604108.
- [9] F. Gelis, “Color Glass Condensate and Glasma”, *Int. J. Mod. Phys. A* **28** (2013) 1330001, arXiv:1211.3327 [hep-ph].
- [10] F. Arleo, R. Kolevato, S. Peigné, and M. Rustamova, “Centrality and p_{\perp} dependence of J/ψ suppression in proton-nucleus collisions from parton energy loss”, *JHEP* **05** (2013) 155, arXiv:1304.0901 [hep-ph].
- [11] E. G. Ferreira, “Excited charmonium suppression in proton–nucleus collisions as a consequence of comovers”, *Phys. Lett. B* **749** (2015) 98–103, arXiv:1411.0549 [hep-ph].
- [12] B. Chen, T. Guo, Y. Liu, and P. Zhuang, “Cold and Hot Nuclear Matter Effects on Charmonium Production in p+Pb Collisions at LHC Energy”, *Phys. Lett. B* **765** (2017) 323–327, arXiv:1607.07927 [nucl-th].
- [13] X. Du and R. Rapp, “In-Medium Charmonium Production in Proton-Nucleus Collisions”, *JHEP* **03** (2019) 015, arXiv:1808.10014 [nucl-th].
- [14] LHCb Collaboration, R. Aaij *et al.*, “Study of J/ψ production and cold nuclear matter effects in pPb collisions at $\sqrt{s_{NN}} = 5$ TeV”, *JHEP* **02** (2014) 072, arXiv:1308.6729 [nucl-ex].
- [15] ALICE Collaboration, J. Adam *et al.*, “Rapidity and transverse-momentum dependence of the inclusive J/ψ nuclear modification factor in p-Pb collisions at $\sqrt{s_{NN}} = 5.02$ TeV”, *JHEP* **06** (2015) 055, arXiv:1503.07179 [nucl-ex].
- [16] ALICE Collaboration, J. Adam *et al.*, “Centrality dependence of inclusive J/ψ production in p-Pb collisions at $\sqrt{s_{NN}} = 5.02$ TeV”, *JHEP* **11** (2015) 127, arXiv:1506.08808 [nucl-ex].

- [17] **ALICE** Collaboration, J. Adam *et al.*, “Measurement of electrons from beauty-hadron decays in p–Pb collisions at $\sqrt{s_{NN}} = 5.02$ TeV and Pb–Pb collisions at $\sqrt{s_{NN}} = 2.76$ TeV”, *JHEP* **07** (2017) 052, arXiv:1609.03898 [nucl-ex].
- [18] **CMS** Collaboration, A. M. Sirunyan *et al.*, “Measurement of prompt and nonprompt J/ψ production in pp and pPb collisions at $\sqrt{s_{NN}} = 5.02$ TeV”, *Eur. Phys. J. C* **77** (2017) 269, arXiv:1702.01462 [nucl-ex].
- [19] **ATLAS** Collaboration, M. Aaboud *et al.*, “Measurement of quarkonium production in proton–lead and proton–proton collisions at 5.02 TeV with the ATLAS detector”, *Eur. Phys. J. C* **78** (2018) 171, arXiv:1709.03089 [nucl-ex].
- [20] **ALICE** Collaboration, S. Acharya *et al.*, “Inclusive, prompt and non-prompt J/ψ production at midrapidity in p–Pb collisions at $\sqrt{s_{NN}} = 5.02$ TeV”, *JHEP* **06** (2022) 011, arXiv:2105.04957 [nucl-ex].
- [21] **CMS** Collaboration, V. Khachatryan *et al.*, “Study of B Meson Production in p+Pb Collisions at $\sqrt{s_{NN}} = 5.02$ TeV Using Exclusive Hadronic Decays”, *Phys. Rev. Lett.* **116** (2016) 032301, arXiv:1508.06678 [nucl-ex].
- [22] **LHCb** Collaboration, R. Aaij *et al.*, “Prompt and nonprompt J/ψ production and nuclear modification in pPb collisions at $\sqrt{s_{NN}} = 8.16$ TeV”, *Phys. Lett. B* **774** (2017) 159–178, arXiv:1706.07122 [hep-ex].
- [23] **ALICE** Collaboration, S. Acharya *et al.*, “Inclusive J/ψ production at forward and backward rapidity in p–Pb collisions at $\sqrt{s_{NN}} = 8.16$ TeV”, *JHEP* **07** (2018) 160, arXiv:1805.04381 [nucl-ex].
- [24] **LHCb** Collaboration, R. Aaij *et al.*, “Measurement of B^+ , B^0 and Λ_b^0 production in pPb collisions at $\sqrt{s_{NN}} = 8.16$ TeV”, *Phys. Rev. D* **99** (2019) 052011, arXiv:1902.05599 [hep-ex].
- [25] **ALICE** Collaboration, K. Aamodt *et al.*, “The ALICE experiment at the CERN LHC”, *JINST* **3** (2008) S08002.
- [26] **ALICE** Collaboration, B. Abelev *et al.*, “Performance of the ALICE Experiment at the CERN LHC”, *Int. J. Mod. Phys. A* **29** (2014) 1430044, arXiv:1402.4476 [nucl-ex].
- [27] **ALICE** Collaboration, K. Aamodt *et al.*, “Alignment of the ALICE Inner Tracking System with cosmic-ray tracks”, *JINST* **5** (2010) P03003, arXiv:1001.0502 [physics.ins-det].
- [28] J. Alme *et al.*, “The ALICE TPC, a large 3-dimensional tracking device with fast readout for ultra-high multiplicity events”, *Nucl. Instrum. Meth. A* **622** (2010) 316–367, arXiv:1001.1950 [physics.ins-det].
- [29] **ALICE** Collaboration, S. Acharya *et al.*, “The ALICE Transition Radiation Detector: construction, operation, and performance”, *Nucl. Instrum. Meth. A* **881** (2018) 88–127, arXiv:1709.02743 [physics.ins-det].
- [30] **ALICE** Collaboration, G. Dellacasa *et al.*, “ALICE technical design report of the photon spectrometer (PHOS)”, tech. rep., 3, 1999. CERN-LHCC-99-004.
- [31] **ALICE** Collaboration, E. Abbas *et al.*, “Performance of the ALICE VZERO system”, *JINST* **8** (2013) P10016, arXiv:1306.3130 [nucl-ex].
- [32] **ALICE** Collaboration, S. Acharya *et al.*, “Inclusive J/ψ production at midrapidity in pp collisions at $\sqrt{s} = 13$ TeV”, *Eur. Phys. J. C* **81** (2021) 1121, arXiv:2108.01906 [nucl-ex].

- [33] **ALICE** Collaboration, S. Acharya *et al.*, “Inclusive J/ψ production at mid-rapidity in pp collisions at $\sqrt{s} = 5.02$ TeV”, *JHEP* **10** (2019) 084, arXiv:1905.07211 [nucl-ex].
- [34] **ALICE** Collaboration, S. Acharya *et al.*, “Prompt and non-prompt J/ψ production cross sections at midrapidity in proton-proton collisions at $\sqrt{s} = 5.02$ and 13 TeV”, *JHEP* **03** (2022) 190, arXiv:2108.02523 [nucl-ex].
- [35] T. Pierog, I. Karpenko, J. M. Katzy, E. Yatsenko, and K. Werner, “EPOS LHC: Test of collective hadronization with data measured at the CERN Large Hadron Collider”, *Phys. Rev. C* **92** (2015) 034906, arXiv:1306.0121 [hep-ph].
- [36] T. Sjostrand, S. Mrenna, and P. Z. Skands, “PYTHIA 6.4 Physics and Manual”, *JHEP* **05** (2006) 026, arXiv:hep-ph/0603175.
- [37] D. J. Lange, “The EvtGen particle decay simulation package”, *Nucl. Instrum. Meth. A* **462** (2001) 152–155.
- [38] E. Barberio and Z. Was, “PHOTOS: A Universal Monte Carlo for QED radiative corrections. Version 2.0”, *Comput. Phys. Commun.* **79** (1994) 291–308.
- [39] R. Brun, F. Bruyant, F. Carminati, S. Giani, M. Maire, A. McPherson, G. Patrick, and L. Urban, *GEANT: Detector Description and Simulation Tool; Oct 1994*. CERN Program Library. CERN, Geneva, 1993. <https://cds.cern.ch/record/1082634>. Long Writeup W5013.
- [40] **Particle Data Group** Collaboration, P. Zyla *et al.*, “Review of Particle Physics”, *PTEP* **2020** (2020) 083C01.
- [41] **ALICE** Collaboration, “ALICE luminosity determination for p-Pb collisions at $\sqrt{s_{NN}} = 8.16$ TeV”, tech. rep., 2018. <https://cds.cern.ch/record/2314660>. ALICE-PUBLIC-2018-002.
- [42] **ALICE** Collaboration, S. Acharya *et al.*, “Measurement of D-meson production at mid-rapidity in pp collisions at $\sqrt{s} = 7$ TeV”, *Eur. Phys. J. C* **77** (2017) 550, arXiv:1702.00766 [hep-ex].
- [43] **ALICE** Collaboration, B. Abelev *et al.*, “Measurement of prompt J/ψ and beauty hadron production cross sections at mid-rapidity in pp collisions at $\sqrt{s} = 7$ TeV”, *JHEP* **11** (2012) 065, arXiv:1205.5880 [hep-ex].
- [44] **ALICE** Collaboration, J. Adam *et al.*, “Inclusive, prompt and non-prompt J/ψ production at mid-rapidity in Pb-Pb collisions at $\sqrt{s_{NN}} = 2.76$ TeV”, *JHEP* **07** (2015) 051, arXiv:1504.07151 [nucl-ex].
- [45] **ALICE** Collaboration, S. Acharya *et al.*, “Prompt and non-prompt J/ψ production and nuclear modification at mid-rapidity in p–Pb collisions at $\sqrt{s_{NN}} = 5.02$ TeV”, *Eur. Phys. J. C* **78** (2018) 466, arXiv:1802.00765 [nucl-ex].
- [46] **ALICE** Collaboration, “Quarkonium signal extraction in ALICE”, tech. rep., 2015. <https://cds.cern.ch/record/2060096>. ALICE-PUBLIC-2015-006.
- [47] **LHCb** Collaboration, R. Aaij *et al.*, “Measurement of b hadron fractions in 13 TeV pp collisions”, *Phys. Rev. D* **100** (2019) 031102, arXiv:1902.06794 [hep-ex].
- [48] **ALICE** Collaboration, B. Abelev *et al.*, “J/ψ polarization in pp collisions at $\sqrt{s} = 7$ TeV”, *Phys. Rev. Lett.* **108** (2012) 082001, arXiv:1111.1630 [hep-ex].
- [49] **LHCb** Collaboration, R. Aaij *et al.*, “Measurement of J/ψ production in pp collisions at $\sqrt{s} = 7$ TeV”, *Eur. Phys. J. C* **71** (2011) 1645, arXiv:1103.0423 [hep-ex].

- [50] **CMS** Collaboration, S. Chatrchyan *et al.*, “Measurement of the Prompt J/ψ and $\psi(2S)$ Polarizations in pp Collisions at $\sqrt{s} = 7$ TeV”, *Phys. Lett. B* **727** (2013) 381–402, arXiv:1307.6070 [hep-ex].
- [51] M. Cacciari, M. Greco, and P. Nason, “The P(T) spectrum in heavy flavor hadroproduction”, *JHEP* **05** (1998) 007, arXiv:hep-ph/9803400 [hep-ph].
- [52] M. Cacciari, S. Frixione, and P. Nason, “The p(T) spectrum in heavy flavor photoproduction”, *JHEP* **03** (2001) 006, arXiv:hep-ph/0102134 [hep-ph].
- [53] M. Cacciari, S. Frixione, N. Houdeau, M. L. Mangano, P. Nason, and G. Ridolfi, “Theoretical predictions for charm and bottom production at the LHC”, *JHEP* **10** (2012) 137, arXiv:1205.6344 [hep-ph].
- [54] **ALICE** Collaboration, B. Abelev *et al.*, “Measurement of electrons from beauty hadron decays in pp collisions at $\sqrt{s} = 7$ TeV”, *Phys. Lett. B* **721** (2013) 13–23, arXiv:1208.1902 [hep-ex]. [Erratum: *Phys.Lett.B* 763, 507–509 (2016)].
- [55] **ALICE** Collaboration, S. Acharya *et al.*, “Measurement of beauty and charm production in pp collisions at $\sqrt{s} = 5.02$ TeV via non-prompt and prompt D mesons”, *JHEP* **05** (2021) 220, arXiv:2102.13601 [nucl-ex].
- [56] F. Bossu, Z. C. del Valle, A. de Falco, M. Gagliardi, S. Grigoryan, and G. Martinez Garcia, “Phenomenological interpolation of the inclusive J/ψ cross section to proton-proton collisions at 2.76 TeV and 5.5 TeV”, arXiv:1103.2394 [nucl-ex].
- [57] **CDF** Collaboration, D. Acosta *et al.*, “Measurement of the J/ψ meson and b –hadron production cross sections in $p\bar{p}$ collisions at $\sqrt{s} = 1960$ GeV”, *Phys. Rev. D* **71** (2005) 032001, arXiv:hep-ex/0412071 [hep-ex].
- [58] **CMS** Collaboration, V. Khachatryan *et al.*, “Prompt and Non-Prompt J/ψ Production in pp Collisions at $\sqrt{s} = 7$ TeV”, *Eur. Phys. J. C* **71** (2011) 1575, arXiv:1011.4193 [hep-ex].
- [59] **ATLAS** Collaboration, G. Aad *et al.*, “Measurement of the differential cross-sections of inclusive, prompt and non-prompt J/ψ production in proton-proton collisions at $\sqrt{s} = 7$ TeV”, *Nucl. Phys. B* **850** (2011) 387–444, arXiv:1104.3038 [hep-ex].
- [60] **LHCb** Collaboration, R. Aaij *et al.*, “Production of J/ψ and Υ mesons in pp collisions at $\sqrt{s} = 8$ TeV”, *JHEP* **06** (2013) 064, arXiv:1304.6977 [hep-ex].
- [61] **ALICE** Collaboration, S. Acharya *et al.*, “Energy dependence of forward-rapidity J/ψ and $\psi(2S)$ production in pp collisions at the LHC”, *Eur. Phys. J. C* **77** (2017) 392, arXiv:1702.00557 [hep-ex].
- [62] **LHCb** Collaboration, R. Aaij *et al.*, “Measurement of forward J/ψ production cross-sections in pp collisions at $\sqrt{s} = 13$ TeV”, *JHEP* **10** (2015) 172, arXiv:1509.00771 [hep-ex]. [Erratum: *JHEP* 05, 063 (2017)].
- [63] **ALICE** Collaboration, S. Acharya *et al.*, “Charm-quark fragmentation fractions and production cross section at midrapidity in pp collisions at the LHC”, *Phys. Rev. D* **105** (2022) L011103, arXiv:2105.06335 [nucl-ex].
- [64] **PHENIX** Collaboration, A. Adare *et al.*, “ J/ψ production versus transverse momentum and rapidity in $p + p$ collisions at $\sqrt{s} = 200$ -GeV”, *Phys. Rev. Lett.* **98** (2007) 232002, arXiv:hep-ex/0611020 [hep-ex].

- [65] ALICE Collaboration, K. Aamodt *et al.*, “Rapidity and transverse momentum dependence of inclusive J/ψ production in pp collisions at $\sqrt{s} = 7$ TeV”, *Phys. Lett.* **B704** (2011) 442–455, arXiv:1105.0380 [hep-ex]. [Erratum: *Phys. Lett.*B718,692(2012)].
- [66] ALICE Collaboration, B. Abelev *et al.*, “Inclusive J/ψ production in pp collisions at $\sqrt{s} = 2.76$ TeV”, *Phys. Lett.* **B718** (2012) 295–306, arXiv:1203.3641 [hep-ex]. [Erratum: *Phys. Lett.*B748,472(2015)].
- [67] ATLAS Collaboration, G. Aad *et al.*, “Measurement of the differential cross-sections of prompt and non-prompt production of J/ψ and ψ(2S) in pp collisions at $\sqrt{s} = 7$ and 8 TeV with the ATLAS detector”, *Eur. Phys. J. C* **76** (2016) 283, arXiv:1512.03657 [hep-ex].
- [68] J.-P. Lansberg and H.-S. Shao, “Towards an automated tool to evaluate the impact of the nuclear modification of the gluon density on quarkonium, D and B meson production in proton–nucleus collisions”, *Eur. Phys. J. C* **77** (2017) 1, arXiv:1610.05382 [hep-ph].
- [69] H.-S. Shao, “HELAC-Onia 2.0: an upgraded matrix-element and event generator for heavy quarkonium physics”, *Comput. Phys. Commun.* **198** (2016) 238–259, arXiv:1507.03435 [hep-ph].
- [70] K. J. Eskola, P. Paakkinen, H. Paukkunen, and C. A. Salgado, “EPPS16: Nuclear parton distributions with LHC data”, *Eur. Phys. J. C* **77** (2017) 163, arXiv:1612.05741 [hep-ph].
- [71] J. L. Albacete *et al.*, “Predictions for p+Pb Collisions at $\sqrt{s_{NN}} = 5$ TeV”, *Int. J. Mod. Phys. E* **22** (2013) 1330007, arXiv:1301.3395 [hep-ph].
- [72] F. Arleo and S. Peigné, “Quarkonium suppression in heavy-ion collisions from coherent energy loss in cold nuclear matter”, *JHEP* **10** (2014) 073, arXiv:1407.5054 [hep-ph].
- [73] J. L. Albacete *et al.*, “Predictions for Cold Nuclear Matter Effects in p+Pb Collisions at $\sqrt{s_{NN}} = 8.16$ TeV”, *Nucl. Phys. A* **972** (2018) 18–85, arXiv:1707.09973 [hep-ph].
- [74] A. Kusina, J.-P. Lansberg, I. Schienbein, and H.-S. Shao, “Gluon Shadowing in Heavy-Flavor Production at the LHC”, *Phys. Rev. Lett.* **121** (2018) 052004, arXiv:1712.07024 [hep-ph].
- [75] K. J. Eskola, P. Paakkinen, H. Paukkunen, and C. A. Salgado, “EPPS16: Nuclear parton distributions with LHC data”, *Eur. Phys. J. C* **77** (2017) 163, arXiv:1612.05741 [hep-ph].
- [76] K. Kovarik *et al.*, “nCTEQ15 - Global analysis of nuclear parton distributions with uncertainties in the CTEQ framework”, *Phys. Rev. D* **93** (2016) 085037, arXiv:1509.00792 [hep-ph].
- [77] Z. Citron *et al.*, “Report from Working Group 5: Future physics opportunities for high-density QCD at the LHC with heavy-ion and proton beams”, *CERN Yellow Rep. Monogr.* **7** (2019) 1159–1410, arXiv:1812.06772 [hep-ph].
- [78] ALICE Collaboration, B. Abelev *et al.*, “Upgrade of the ALICE Experiment: Letter Of Intent”, *J. Phys. G* **41** (2014) 087001.
- [79] ATLAS Collaboration, G. Aad *et al.*, “Measurement of differential J/ψ production cross sections and forward-backward ratios in p + Pb collisions with the ATLAS detector”, *Phys. Rev. C* **92** (2015) 034904, arXiv:1505.08141 [hep-ex].
- [80] P. Duventäster, T. Ježo, M. Klasen, K. Kovařík, A. Kusina, K. F. Muzakka, F. I. Olness, R. Ruiz, I. Schienbein, and J. Y. Yu, “Impact of heavy quark and quarkonium data on nuclear gluon PDFs”, *Phys. Rev. D* **105** (2022) 114043, arXiv:2204.09982 [hep-ph].








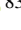
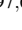


- [81] C. H. Kom, A. Kulesza, and W. J. Stirling, “Pair Production of J/ψ as a Probe of Double Parton Scattering at LHCb”, *Phys. Rev. Lett.* **107** (2011) 082002, arXiv:1105.4186 [hep-ph].
- [82] B. A. Kniehl, G. Kramer, I. Schienbein, and H. Spiesberger, “Inclusive $D^{*\pm}$ production in p \bar{p} collisions with massive charm quarks”, *Phys. Rev. D* **71** (2005) 014018, arXiv:hep-ph/0410289.

A The ALICE Collaboration

S. Acharya ¹²⁵, D. Adamová ⁸⁶, A. Adler⁶⁹, G. Aglieri Rinella ³², M. Agnello ²⁹, N. Agrawal ⁵⁰, Z. Ahammed ¹³², S. Ahmad ¹⁵, S.U. Ahn ⁷⁰, I. Ahuja ³⁷, A. Akindinov ¹⁴⁰, M. Al-Turany ⁹⁷, D. Aleksandrov ¹⁴⁰, B. Alessandro ⁵⁵, H.M. Alfanda ⁶, R. Alfaro Molina ⁶⁶, B. Ali ¹⁵, A. Alici ²⁵, N. Alizadehvandchali ¹¹⁴, A. Alkin ³², J. Alme ²⁰, G. Alocco ⁵¹, T. Alt ⁶³, I. Altsybeev ¹⁴⁰, M.N. Anaam ⁶, C. Andrei ⁴⁵, A. Andronic ¹³⁵, V. Anguelov ⁹⁴, F. Antinori ⁵³, P. Antonioli ⁵⁰, N. Apadula ⁷⁴, L. Aphecetche ¹⁰³, H. Appelshäuser ⁶³, C. Arata ⁷³, S. Arcelli ²⁵, M. Aresti ⁵¹, R. Arnaldi ⁵⁵, J.G.M.C.A. Arneiro ¹¹⁰, I.C. Arsene ¹⁹, M. Arslanok ¹³⁷, A. Augustinus ³², R. Averbeck ⁹⁷, M.D. Azmi ¹⁵, A. Badalà ⁵², J. Bae ¹⁰⁴, Y.W. Baek ⁴⁰, X. Bai ¹¹⁸, R. Bailhache ⁶³, Y. Bailung ⁴⁷, A. Balbino ²⁹, A. Baldisseri ¹²⁸, B. Balis ², D. Banerjee ⁴, Z. Banoo ⁹¹, R. Barbera ²⁶, F. Barile ³¹, L. Barioglio ⁹⁵, M. Barlou⁷⁸, G.G. Barnaföldi ¹³⁶, L.S. Barnby ⁸⁵, V. Barret ¹²⁵, L. Barreto ¹¹⁰, C. Bartels ¹¹⁷, K. Barth ³², E. Bartsch ⁶³, N. Bastid ¹²⁵, S. Basu ⁷⁵, G. Batigne ¹⁰³, D. Battistini ⁹⁵, B. Batyunya ¹⁴¹, D. Bauri⁴⁶, J.L. Bazo Alba ¹⁰¹, I.G. Bearden ⁸³, C. Beattie ¹³⁷, P. Becht ⁹⁷, D. Behera ⁴⁷, I. Belikov ¹²⁷, A.D.C. Bell Hechavarria ¹³⁵, F. Bellini ²⁵, R. Bellwied ¹¹⁴, S. Belokurova ¹⁴⁰, V. Belyaev ¹⁴⁰, G. Bencedi ¹³⁶, S. Beole ²⁴, A. Bercuci ⁴⁵, Y. Berdnikov ¹⁴⁰, A. Berdnikova ⁹⁴, L. Bergmann ⁹⁴, M.G. Besoiu ⁶², L. Betev ³², P.P. Bhaduri ¹³², A. Bhasin ⁹¹, M.A. Bhat ⁴, B. Bhattacharjee ⁴¹, L. Bianchi ²⁴, N. Bianchi ⁴⁸, J. Bielčik ³⁵, J. Bielčiková ⁸⁶, J. Biernat ¹⁰⁷, A.P. Bigot ¹²⁷, A. Bilandzic ⁹⁵, G. Biro ¹³⁶, S. Biswas ⁴, N. Bize ¹⁰³, J.T. Blair ¹⁰⁸, D. Blau ¹⁴⁰, M.B. Blidaru ⁹⁷, N. Bluhme³⁸, C. Blume ⁶³, G. Boca ^{21,54}, F. Bock ⁸⁷, T. Bodova ²⁰, A. Bogdanov¹⁴⁰, S. Boi ²², J. Bok ⁵⁷, L. Boldizsár ¹³⁶, A. Bolozdynya ¹⁴⁰, M. Bombara ³⁷, P.M. Bond ³², G. Bonomi ^{131,54}, H. Borel ¹²⁸, A. Borissov ¹⁴⁰, A.G. Borquez Carcamo ⁹⁴, H. Bossi ¹³⁷, E. Botta ²⁴, Y.E.M. Bouziani ⁶³, L. Bratrud ⁶³, P. Braun-Munzinger ⁹⁷, M. Bregant ¹¹⁰, M. Broz ³⁵, G.E. Bruno ^{96,31}, M.D. Buckland ²³, D. Budnikov ¹⁴⁰, H. Buesching ⁶³, S. Bufalino ²⁹, O. Bugnon¹⁰³, P. Buhler ¹⁰², Z. Buthelezi ^{67,121}, S.A. Bysiak¹⁰⁷, M. Cai ⁶, H. Caines ¹³⁷, A. Caliva ⁹⁷, E. Calvo Villar ¹⁰¹, J.M.M. Camacho ¹⁰⁹, P. Camerini ²³, F.D.M. Canedo ¹¹⁰, M. Carabas ¹²⁴, A.A. Carballo ³², F. Carnesecchi ³², R. Caron ¹²⁶, L.A.D. Carvalho ¹¹⁰, J. Castillo Castellanos ¹²⁸, F. Catalano ^{24,29}, C. Ceballos Sanchez ¹⁴¹, I. Chakaberia ⁷⁴, P. Chakraborty ⁴⁶, S. Chandra ¹³², S. Chapeland ³², M. Chartier ¹¹⁷, S. Chattopadhyay ¹³², S. Chattopadhyay ⁹⁹, T.G. Chavez ⁴⁴, T. Cheng ^{97,6}, C. Cheshkov ¹²⁶, B. Cheynis ¹²⁶, V. Chibante Barroso ³², D.D. Chinellato ¹¹¹, E.S. Chizzali ^{11,95}, J. Cho ⁵⁷, S. Cho ⁵⁷, P. Chochula ³², P. Christakoglou ⁸⁴, C.H. Christensen ⁸³, P. Christiansen ⁷⁵, T. Chujo ¹²³, M. Ciacco ²⁹, C. Cicalo ⁵¹, F. Cindolo ⁵⁰, M.R. Ciupek⁹⁷, G. Clai^{III,50}, F. Colamaria ⁴⁹, J.S. Colburn¹⁰⁰, D. Colella ^{96,31}, M. Colocci ³², M. Concas ^{IV,55}, G. Conesa Balbastre ⁷³, Z. Conesa del Valle ⁷², G. Contin ²³, J.G. Contreras ³⁵, M.L. Coquet ¹²⁸, T.M. Cormier^{I,87}, P. Cortese ^{130,55}, M.R. Cosentino ¹¹², F. Costa ³², S. Costanza ^{21,54}, C. Cot ⁷², J. Crković ⁹⁴, P. Crochet ¹²⁵, R. Cruz-Torres ⁷⁴, E. Cuautle⁶⁴, P. Cui ⁶, A. Dainese ⁵³, M.C. Danisch ⁹⁴, A. Danu ⁶², P. Das ⁸⁰, P. Das ⁴, S. Das ⁴, A.R. Dash ¹³⁵, S. Dash ⁴⁶, A. De Caro ²⁸, G. de Cataldo ⁴⁹, J. de Cuveland³⁸, A. De Falco ²², D. De Gruttola ²⁸, N. De Marco ⁵⁵, C. De Martin ²³, S. De Pasquale ²⁸, S. Deb ⁴⁷, R.J. Debski ², K.R. Deja¹³³, R. Del Grande ⁹⁵, L. Dello Stritto ²⁸, W. Deng ⁶, P. Dhankher ¹⁸, D. Di Bari ³¹, A. Di Mauro ³², R.A. Diaz ^{141,7}, T. Dietel ¹¹³, Y. Ding ^{126,6}, R. Divià ³², D.U. Dixit ¹⁸, Ø. Djuvsland²⁰, U. Dmitrieva ¹⁴⁰, A. Dobrin ⁶², B. Dönigus ⁶³, J.M. Dubinski¹³³, A. Dubla ⁹⁷, S. Dudi ⁹⁰, P. Dupieux ¹²⁵, M. Durkac¹⁰⁶, N. Dzalaiova¹², T.M. Eder ¹³⁵, R.J. Ehlers ⁸⁷, V.N. Eikeland²⁰, F. Eisenhut ⁶³, D. Elia ⁴⁹, B. Erasmus ¹⁰³, F. Ercolessi ²⁵, F. Erhardt ⁸⁹, M.R. Ersdal²⁰, B. Espagnon ⁷², G. Eulisse ³², D. Evans ¹⁰⁰, S. Evdokimov ¹⁴⁰, L. Fabbietti ⁹⁵, M. Faggin ²⁷, J. Faivre ⁷³, F. Fan ⁶, W. Fan ⁷⁴, A. Fantoni ⁴⁸, M. Fasel ⁸⁷, P. Fedchio²⁹, A. Feliciello ⁵⁵, G. Feofilov ¹⁴⁰, A. Fernández Téllez ⁴⁴, L. Ferrandi ¹¹⁰, M.B. Ferrer ³², A. Ferrero ¹²⁸, C. Ferrero ⁵⁵, A. Ferretti ²⁴, V.J.G. Feuillard ⁹⁴, V. Filova³⁵, D. Finogeev ¹⁴⁰, F.M. Fionda ⁵¹, F. Flor ¹¹⁴, A.N. Flores ¹⁰⁸, S. Foertsch ⁶⁷, I. Fokin ⁹⁴, S. Fokin ¹⁴⁰, E. Fragiaco ⁵⁶, E. Frajna ¹³⁶, U. Fuchs ³², N. Funicello ²⁸, C. Furget ⁷³, A. Furs ¹⁴⁰, T. Fusayasu ⁹⁸, J.J. Gaardhøje ⁸³, M. Gagliardi ²⁴, A.M. Gago ¹⁰¹, C.D. Galvan ¹⁰⁹, D.R. Gangadharan ¹¹⁴, P. Ganoti ⁷⁸, C. Garabatos ⁹⁷, J.R.A. Garcia ⁴⁴, E. Garcia-Solis ⁹, K. Garg ¹⁰³, C. Gargiulo ³², A. Garibli⁸¹, K. Garner¹³⁵, P. Gasik ⁹⁷, A. Gautam ¹¹⁶, M.B. Gay Ducati ⁶⁵, M. Germain ¹⁰³, A. Ghimouz¹²³, C. Ghosh¹³², M. Giacalone ^{50,25}, P. Giubellino ^{97,55}, P. Giubilato ²⁷, A.M.C. Glaenger ¹²⁸, P. Glässel ⁹⁴, E. Glimos¹²⁰, D.J.Q. Goh⁷⁶, V. Gonzalez ¹³⁴, L.H. González-Trueba ⁶⁶, S. Gorbunov³⁸, M. Gorgon ², S. Gotovac³³, V. Grabski ⁶⁶, L.K. Graczykowski ¹³³, E. Grecka ⁸⁶, A. Grelli ⁵⁸, C. Grigoras ³², V. Grigoriev ¹⁴⁰, S. Grigoryan ^{141,1}, F. Grosa ³², J.F. Grosse-Oetringhaus ³², R. Grosso ⁹⁷, D. Grund ³⁵, G.G. Guardiano ¹¹¹, R. Guernane ⁷³, M. Guilbaud ¹⁰³, K. Gulbrandsen ⁸³, T. Gundem ⁶³, T. Gunji ¹²², W. Guo ⁶,

A. Gupta⁹¹, R. Gupta⁹¹, S.P. Guzman⁴⁴, L. Gyulai¹³⁶, M.K. Habib⁹⁷, C. Hadjidakis⁷², F.U. Haider⁹¹, H. Hamagaki⁷⁶, A. Hamdi⁷⁴, M. Hamid⁶, Y. Han¹³⁸, R. Hannigan¹⁰⁸, M.R. Haque¹³³, J.W. Harris¹³⁷, A. Harton⁹, H. Hassan⁸⁷, D. Hatzifotiadou⁵⁰, P. Hauer⁴², L.B. Havener¹³⁷, S.T. Heckel⁹⁵, E. Hellbär⁹⁷, H. Helstrup³⁴, M. Hemmer⁶³, T. Herman³⁵, G. Herrera Corral⁸, F. Herrmann¹³⁵, S. Herrmann¹²⁶, K.F. Hetland³⁴, B. Heybeck⁶³, H. Hillemanns³², C. Hills¹¹⁷, B. Hippolyte¹²⁷, F.W. Hoffmann⁶⁹, B. Hofman⁵⁸, B. Hohlweger⁸⁴, G.H. Hong¹³⁸, M. Horst⁹⁵, A. Horzyk², R. Hosokawa¹⁴, Y. Hou⁶, P. Hristov³², C. Hughes¹²⁰, P. Huhn⁶³, L.M. Huhta¹¹⁵, C.V. Hulse⁷², T.J. Humanic⁸⁸, A. Hutson¹¹⁴, D. Hutter³⁸, J.P. Iddon¹¹⁷, R. Ilkaev¹⁴⁰, H. Ilyas¹³, M. Inaba¹²³, G.M. Innocenti³², M. Ippolitov¹⁴⁰, A. Isakov⁸⁶, T. Isidori¹¹⁶, M.S. Islam⁹⁹, M. Ivanov¹², M. Ivanov⁹⁷, V. Ivanov¹⁴⁰, M. Jablonski², B. Jacak⁷⁴, N. Jacazio³², P.M. Jacobs⁷⁴, S. Jadlovská¹⁰⁶, J. Jadlovsky¹⁰⁶, S. Jaelani⁸², L. Jaffe³⁸, C. Jahnke¹¹¹, M.J. Jakubowska¹³³, M.A. Janik¹³³, T. Janson⁶⁹, M. Jercic⁸⁹, S. Jia¹⁰, A.A.P. Jimenez⁶⁴, F. Jonas⁸⁷, J.M. Jowett^{32,97}, J. Jung⁶³, M. Jung⁶³, A. Junique³², A. Jusko¹⁰⁰, M.J. Kabus^{32,133}, J. Kaewjai¹⁰⁵, P. Kalinak⁵⁹, A.S. Kalteyer⁹⁷, A. Kalweit³², V. Kaplin¹⁴⁰, A. Karasu Uysal⁷¹, D. Karatovic⁸⁹, O. Karavichev¹⁴⁰, T. Karavicheva¹⁴⁰, P. Karczmarczyk¹³³, E. Karpechev¹⁴⁰, U. Keschull⁶⁹, R. Keidel¹³⁹, D.L.D. Keijdener⁵⁸, M. Keil³², B. Ketzer⁴², A.M. Khan⁶, S. Khan¹⁵, A. Khanzadeev¹⁴⁰, Y. Kharlov¹⁴⁰, A. Khatun^{116,15}, A. Khuntia¹⁰⁷, M.B. Kidson¹¹³, B. Kileng³⁴, B. Kim¹⁶, C. Kim¹⁶, D.J. Kim¹¹⁵, E.J. Kim⁶⁸, J. Kim¹³⁸, J.S. Kim⁴⁰, J. Kim⁶⁸, M. Kim^{18,94}, S. Kim¹⁷, T. Kim¹³⁸, K. Kimura⁹², S. Kirsch⁶³, I. Kisel³⁸, S. Kiselev¹⁴⁰, A. Kisiel¹³³, J.P. Kitowski², J.L. Klay⁵, J. Klein³², S. Klein⁷⁴, C. Klein-Bösing¹³⁵, M. Kleiner⁶³, T. Klemenz⁹⁵, A. Kluge³², A.G. Knospe¹¹⁴, C. Kobdaj¹⁰⁵, T. Kollegger⁹⁷, A. Kondratyev¹⁴¹, N. Kondratyeva¹⁴⁰, E. Kondratyuk¹⁴⁰, J. Konig⁶³, S.A. Konigstorfer⁹⁵, P.J. Konopka³², G. Kornakov¹³³, S.D. Koryciak², A. Kotliarov⁸⁶, V. Kovalenko¹⁴⁰, M. Kowalski¹⁰⁷, V. Kozhuharov³⁶, I. Králik⁵⁹, A. Kravčáková³⁷, L. Kreis⁹⁷, M. Krivda^{100,59}, F. Krizek⁸⁶, K. Krizkova Gajdosova³⁵, M. Kroesen⁹⁴, M. Krüger⁶³, D.M. Krupova³⁵, E. Kryshen¹⁴⁰, V. Kučera³², C. Kuhn¹²⁷, P.G. Kuijjer⁸⁴, T. Kumaoka¹²³, D. Kumar¹³², L. Kumar⁹⁰, N. Kumar⁹⁰, S. Kumar³¹, S. Kundu³², P. Kurashvili⁷⁹, A. Kurepin¹⁴⁰, A.B. Kurepin¹⁴⁰, A. Kuryakin¹⁴⁰, S. Kuschpil⁸⁶, J. Kvapil¹⁰⁰, M.J. Kweon⁵⁷, J.Y. Kwon⁵⁷, Y. Kwon¹³⁸, S.L. La Pointe³⁸, P. La Rocca²⁶, Y.S. Lai⁷⁴, A. Lakrathok¹⁰⁵, M. Lamanna³², R. Langoy¹¹⁹, P. Larionov³², E. Laudi³², L. Lautner^{32,95}, R. Lavicka¹⁰², T. Lazareva¹⁴⁰, R. Lea^{131,54}, H. Lee¹⁰⁴, G. Legras¹³⁵, J. Lehrbach³⁸, R.C. Lemmon⁸⁵, I. León Monzón¹⁰⁹, M.M. Lesch⁹⁵, E.D. Lesser¹⁸, M. Lettrich⁹⁵, P. Lévai¹³⁶, X. Li¹⁰, X.L. Li⁶, J. Lien¹¹⁹, R. Lietava¹⁰⁰, I. Likmeta¹¹⁴, B. Lim^{24,16}, S.H. Lim¹⁶, V. Lindenstruth³⁸, A. Lindner⁴⁵, C. Lippmann⁹⁷, A. Liu¹⁸, D.H. Liu⁶, J. Liu¹¹⁷, I.M. Lofnes²⁰, C. Loizides⁸⁷, S. Lokos¹⁰⁷, J. Lomker⁵⁸, P. Loncar³³, J.A. Lopez⁹⁴, X. Lopez¹²⁵, E. López Torres⁷, P. Lu^{97,118}, J.R. Luhder¹³⁵, M. Lunardon²⁷, G. Luparello⁵⁶, Y.G. Ma³⁹, A. Maevskaya¹⁴⁰, M. Mager³², T. Mahmoud⁴², A. Maire¹²⁷, M.V. Makariev³⁶, M. Malaev¹⁴⁰, G. Malfattore²⁵, N.M. Malik⁹¹, Q.W. Malik¹⁹, S.K. Malik⁹¹, L. Malinina^{VII,141}, D. Mal'Kevich¹⁴⁰, D. Mallick⁸⁰, N. Mallick⁴⁷, G. Mandaglio^{30,52}, V. Manko¹⁴⁰, F. Manso¹²⁵, V. Manzari⁴⁹, Y. Mao⁶, G.V. Margagliotti²³, A. Margotti⁵⁰, A. Marín⁹⁷, C. Markert¹⁰⁸, P. Martinengo³², J.L. Martínez¹¹⁴, M.I. Martínez⁴⁴, G. Martínez García¹⁰³, S. Masciocchi⁹⁷, M. Maserà²⁴, A. Masoni⁵¹, L. Massacrier⁷², A. Mastroserio^{129,49}, O. Matonoha⁷⁵, P.F.T. Matuoka¹¹⁰, A. Matyja¹⁰⁷, C. Mayer¹⁰⁷, A.L. Mazuecos³², F. Mazzaschi²⁴, M. Mazzilli³², J.E. Mdhuli¹²¹, A.F. Mechler⁶³, Y. Melikyan^{43,140}, A. Menchaca-Rocha⁶⁶, E. Meninno^{102,28}, A.S. Menon¹¹⁴, M. Meres¹², S. Mhlanga^{113,67}, Y. Miake¹²³, L. Micheletti⁵⁵, L.C. Migliorin¹²⁶, D.L. Mihaylov⁹⁵, K. Mikhaylov^{141,140}, A.N. Mishra¹³⁶, D. Miśkowiec⁹⁷, A. Modak⁴, A.P. Mohanty⁵⁸, B. Mohanty⁸⁰, M. Mohisin Khan^{V,15}, M.A. Molander⁴³, Z. Moravcova⁸³, C. Mordasini⁹⁵, D.A. Moreira De Godoy¹³⁵, I. Morozov¹⁴⁰, A. Morsch³², T. Mrnjavac³², V. Muccifora⁴⁸, S. Muhuri¹³², J.D. Mulligan⁷⁴, A. Mulliri²², M.G. Munhoz¹¹⁰, R.H. Munzer⁶³, H. Murakami¹²², S. Murray¹¹³, L. Musa³², J. Musinsky⁵⁹, J.W. Myrcha¹³³, B. Naik¹²¹, A.I. Nambrath¹⁸, B.K. Nandi⁴⁶, R. Nania⁵⁰, E. Nappi⁴⁹, A.F. Nassirpour⁷⁵, A. Nath⁹⁴, C. Nattrass¹²⁰, M.N. Naydenov³⁶, A. Neagu¹⁹, A. Negru¹²⁴, L. Nellen⁶⁴, S.V. Nesbo³⁴, G. Neskovic³⁸, D. Nesterov¹⁴⁰, B.S. Nielsen⁸³, E.G. Nielsen⁸³, S. Nikolaev¹⁴⁰, S. Nikulin¹⁴⁰, V. Nikulin¹⁴⁰, F. Noferini⁵⁰, S. Noh¹¹, P. Nomokonov¹⁴¹, J. Norman¹¹⁷, N. Novitzky¹²³, P. Nowakowski¹³³, A. Nyanin¹⁴⁰, J. Nystrand²⁰, M. Ogino⁷⁶, A. Ohlson⁷⁵, V.A. Okorokov¹⁴⁰, J. Oleniacz¹³³, A.C. Oliveira Da Silva¹²⁰, M.H. Oliver¹³⁷, A. Onnerstad¹¹⁵, C. Oppedisano⁵⁵, A. Ortiz Velasquez⁶⁴, J. Otwinowski¹⁰⁷, M. Oya⁹², K. Oyama⁷⁶, Y. Pachmayer⁹⁴, S. Padhan⁴⁶, D. Pagano^{131,54}, G. Paic⁶⁴, A. Palasciano⁴⁹, S. Panebianco¹²⁸,

H. Park ¹²³, H. Park ¹⁰⁴, J. Park ⁵⁷, J.E. Parkkila ³², R.N. Patra ⁹¹, B. Paul ²², H. Pei ⁶,
T. Peitzmann ⁵⁸, X. Peng ⁶, M. Pennisi ²⁴, L.G. Pereira ⁶⁵, D. Peresunko ¹⁴⁰, G.M. Perez ⁷,
S. Perrin ¹²⁸, Y. Pestov ¹⁴⁰, V. Petráček ³⁵, V. Petrov ¹⁴⁰, M. Petrovici ⁴⁵, R.P. Pezzi ^{103,65}, S. Piano ⁵⁶,
M. Pikna ¹², P. Pillot ¹⁰³, O. Pinazza ^{50,32}, L. Pinsky ¹¹⁴, C. Pinto ⁹⁵, S. Pisano ⁴⁸, M. Płoskoń ⁷⁴,
M. Planinic ⁸⁹, F. Pliquett ⁶³, M.G. Poghosyan ⁸⁷, B. Polichtchouk ¹⁴⁰, S. Politano ²⁹, N. Poljak ⁸⁹,
A. Pop ⁴⁵, S. Porteboeuf-Houssais ¹²⁵, V. Pozdniakov ¹⁴¹, K.K. Pradhan ⁴⁷, S.K. Prasad ⁴, S. Prasad ⁴⁷,
R. Preghenella ⁵⁰, F. Prino ⁵⁵, C.A. Pruneau ¹³⁴, I. Pshenichnov ¹⁴⁰, M. Puccio ³², S. Pucillo ²⁴,
Z. Pugelova ¹⁰⁶, S. Qiu ⁸⁴, L. Quaglia ²⁴, R.E. Quishpe ¹¹⁴, S. Ragoni ^{14,100}, A. Rakotozafindrabe ¹²⁸,
L. Ramello ^{130,55}, F. Rami ¹²⁷, S.A.R. Ramirez ⁴⁴, T.A. Rancien ⁷³, M. Rasa ²⁶, S.S. Räsänen ⁴³,
R. Rath ⁵⁰, M.P. Rauch ²⁰, I. Ravasenga ⁸⁴, K.F. Read ^{87,120}, C. Reckziegel ¹¹², A.R. Redelbach ³⁸,
K. Redlich ^{VI,79}, C.A. Retz ⁹⁷, A. Rehman ²⁰, F. Reidt ³², H.A. Reme-Ness ³⁴, Z. Rescakova ³⁷,
K. Reygiers ⁹⁴, A. Riabov ¹⁴⁰, V. Riabov ¹⁴⁰, R. Ricci ²⁸, M. Richter ¹⁹, A.A. Riedel ⁹⁵,
W. Riegler ³², C. Ristea ⁶², M. Rodríguez Cahuantzi ⁴⁴, K. Røed ¹⁹, R. Rogalev ¹⁴⁰, E. Rogochaya ¹⁴¹,
T.S. Rogoschinski ⁶³, D. Rohr ³², D. Röhrich ²⁰, P.F. Rojas ⁴⁴, S. Rojas Torres ³⁵, P.S. Rokita ¹³³,
G. Romanenko ¹⁴¹, F. Ronchetti ⁴⁸, A. Rosano ^{30,52}, E.D. Rosas ⁶⁴, K. Roslon ¹³³, A. Rossi ⁵³,
A. Roy ⁴⁷, S. Roy ⁴⁶, N. Rubini ²⁵, O.V. Rueda ^{114,75}, D. Ruggiano ¹³³, R. Rui ²³, B. Rumyantsev ¹⁴¹,
P.G. Russek ², R. Russo ⁸⁴, A. Rustamov ⁸¹, E. Ryabinkin ¹⁴⁰, Y. Ryabov ¹⁴⁰, A. Rybicki ¹⁰⁷,
H. Rytkonen ¹¹⁵, W. Rzesza ¹³³, O.A.M. Saarimaki ⁴³, R. Sadek ¹⁰³, S. Sadhu ³¹, S. Sadovsky ¹⁴⁰,
J. Saetre ²⁰, K. Šafařík ³⁵, S.K. Saha ⁴, S. Saha ⁸⁰, B. Sahoo ⁴⁶, R. Sahoo ⁴⁷, S. Sahoo ⁶⁰, D. Sahu ⁴⁷,
P.K. Sahu ⁶⁰, J. Saini ¹³², K. Sajdakova ³⁷, S. Sakai ¹²³, M.P. Salvan ⁹⁷, S. Sambyal ⁹¹, I. Sanna ^{32,95},
T.B. Saramela ¹¹⁰, D. Sarkar ¹³⁴, N. Sarkar ¹³², P. Sarma ⁴¹, V. Sarritzu ²², V.M. Sarti ⁹⁵, M.H.P. Sas ¹³⁷,
J. Schambach ⁸⁷, H.S. Scheid ⁶³, C. Schiaua ⁴⁵, R. Schicker ⁹⁴, A. Schmah ⁹⁴, C. Schmidt ⁹⁷,
H.R. Schmidt ⁹³, M.O. Schmidt ³², M. Schmidt ⁹³, N.V. Schmidt ⁸⁷, A.R. Schmier ¹²⁰, R. Schotter ¹²⁷,
A. Schröter ³⁸, J. Schukraft ³², K. Schwarz ⁹⁷, K. Schweda ⁹⁷, G. Scioli ²⁵, E. Scomparin ⁵⁵,
J.E. Seger ¹⁴, Y. Sekiguchi ¹²², D. Sekihata ¹²², I. Selyuzhenkov ^{97,140}, S. Senyukov ¹²⁷, J.J. Seo ⁵⁷,
D. Serebryakov ¹⁴⁰, L. Šerkšnytė ⁹⁵, A. Sevcenco ⁶², T.J. Shaba ⁶⁷, A. Shabetai ¹⁰³, R. Shahoyan ³²,
A. Shangaraev ¹⁴⁰, A. Sharma ⁹⁰, B. Sharma ⁹¹, D. Sharma ⁴⁶, H. Sharma ¹⁰⁷, M. Sharma ⁹¹,
S. Sharma ⁷⁶, S. Sharma ⁹¹, U. Sharma ⁹¹, A. Shatat ⁷², O. Sheibani ¹¹⁴, K. Shigaki ⁹², M. Shimomura ⁷⁷,
J. Shin ¹¹, S. Shirinkin ¹⁴⁰, Q. Shou ³⁹, Y. Sibiriak ¹⁴⁰, S. Siddhanta ⁵¹, T. Siemiarczuk ⁷⁹,
T.F. Silva ¹¹⁰, D. Silvermyr ⁷⁵, T. Simantathammakul ¹⁰⁵, R. Simeonov ³⁶, B. Singh ⁹¹, B. Singh ⁹⁵,
R. Singh ⁸⁰, R. Singh ⁹¹, R. Singh ⁴⁷, S. Singh ¹⁵, V.K. Singh ¹³², V. Singhal ¹³², T. Sinha ⁹⁹,
B. Sitar ¹², M. Sitta ^{130,55}, T.B. Skaali ¹⁹, G. Skorodumovs ⁹⁴, M. Slupecki ⁴³, N. Smirnov ¹³⁷,
R.J.M. Snellings ⁵⁸, E.H. Solheim ¹⁹, J. Song ¹¹⁴, A. Songmoolnak ¹⁰⁵, F. Soramel ²⁷, R. Spijkers ⁸⁴,
I. Sputowska ¹⁰⁷, J. Staa ⁷⁵, J. Stachel ⁹⁴, I. Stan ⁶², P.J. Steffanic ¹²⁰, S.F. Stiefelmaier ⁹⁴,
D. Stocco ¹⁰³, I. Storehaug ¹⁹, P. Stratmann ¹³⁵, S. Strazzi ²⁵, C.P. Stylianidis ⁸⁴, A.A.P. Suaide ¹¹⁰,
C. Suire ⁷², M. Sukhanov ¹⁴⁰, M. Suljic ³², R. Sultanov ¹⁴⁰, V. Sumberia ⁹¹, S. Sumowidagdo ⁸²,
S. Swain ⁶⁰, I. Szarka ¹², M. Szymkowski ¹³³, S.F. Taghavi ⁹⁵, G. Taillepied ⁹⁷, J. Takahashi ¹¹¹,
G.J. Tambave ²⁰, S. Tang ^{125,6}, Z. Tang ¹¹⁸, J.D. Tapia Takaki ¹¹⁶, N. Tapus ¹²⁴, L.A. Tarasovicova ¹³⁵,
M.G. Tarzila ⁴⁵, G.F. Tassielli ³¹, A. Tauro ³², G. Tejeda Muñoz ⁴⁴, A. Telesca ³², L. Terlizzi ²⁴,
C. Terrevoli ¹¹⁴, G. Tersimonov ³, S. Thakur ⁴, D. Thomas ¹⁰⁸, A. Tikhonov ¹⁴⁰, A.R. Timmins ¹¹⁴,
M. Tkacik ¹⁰⁶, T. Tkacik ¹⁰⁶, A. Toia ⁶³, R. Tokumoto ⁹², N. Topilskaya ¹⁴⁰, M. Toppi ⁴⁸,
F. Torres-Acosta ¹⁸, T. Tork ⁷², A.G. Torres Ramos ³¹, A. Trifiró ^{30,52}, A.S. Triolo ^{30,52}, S. Tripathy ⁵⁰,
T. Tripathy ⁴⁶, S. Trogolo ³², V. Trubnikov ³, W.H. Trzaska ¹¹⁵, T.P. Trzcinski ¹³³, A. Tumkin ¹⁴⁰,
R. Turrisi ⁵³, T.S. Tveter ¹⁹, K. Ullaland ²⁰, B. Ulukutlu ⁹⁵, A. Uras ¹²⁶, M. Urioni ^{54,131},
G.L. Usai ²², M. Vala ³⁷, N. Valle ²¹, L.V.R. van Doremalen ⁵⁸, M. van Leeuwen ⁸⁴, C.A. van Veen ⁹⁴,
R.J.G. van Weelden ⁸⁴, P. Vande Vyvre ³², D. Varga ¹³⁶, Z. Varga ¹³⁶, M. Vasileiou ⁷⁸, A. Vasiliev ¹⁴⁰,
O. Vázquez Doce ⁴⁸, V. Vechernin ¹⁴⁰, E. Vercellin ²⁴, S. Vergara Limón ⁴⁴, L. Vermunt ⁹⁷,
R. Vértesi ¹³⁶, M. Verweij ⁵⁸, L. Vickovic ³³, Z. Vilakazi ¹²¹, O. Villalobos Baillie ¹⁰⁰, A. Villani ²³,
G. Vino ⁴⁹, A. Vinogradov ¹⁴⁰, T. Virgili ²⁸, V. Vislavicius ⁷⁵, A. Vodopyanov ¹⁴¹, B. Volkel ³²,
M.A. Völkl ⁹⁴, K. Voloshin ¹⁴⁰, S.A. Voloshin ¹³⁴, G. Volpe ³¹, B. von Haller ³², I. Vorobyev ⁹⁵,
N. Vozniuk ¹⁴⁰, J. Vrláková ³⁷, C. Wang ³⁹, D. Wang ³⁹, Y. Wang ³⁹, A. Wegrzynek ³², F.T. Weiglhofer ³⁸,
S.C. Wenzel ³², J.P. Wessels ¹³⁵, S.L. Weyhmiller ¹³⁷, J. Wiechula ⁶³, J. Wikne ¹⁹, G. Wilk ⁷⁹,
J. Wilkinson ⁹⁷, G.A. Willems ¹³⁵, B. Windelband ⁹⁴, M. Winn ¹²⁸, J.R. Wright ¹⁰⁸, W. Wu ³⁹, Y. Wu ¹¹⁸,
R. Xu ⁶, A. Yadav ⁴², A.K. Yadav ¹³², S. Yalcin ⁷¹, Y. Yamaguchi ⁹², S. Yang ²⁰, S. Yano ⁹², Z. Yin ⁶,
I.-K. Yoo ¹⁶, J.H. Yoon ⁵⁷, S. Yuan ²⁰, A. Yuncu ⁹⁴, V. Zaccolo ²³, C. Zampolli ³², F. Zanone ⁹⁴,
N. Zardoshti ^{32,100}, A. Zarochentsev ¹⁴⁰, P. Závada ⁶¹, N. Zaviyalov ¹⁴⁰, M. Zhalov ¹⁴⁰, B. Zhang ⁶,

L. Zhang ³⁹, S. Zhang ³⁹, X. Zhang ⁶, Y. Zhang¹¹⁸, Z. Zhang ⁶, M. Zhao ¹⁰, V. Zherebchevskii ¹⁴⁰,
Y. Zhi¹⁰, D. Zhou ⁶, Y. Zhou ⁸³, J. Zhu ^{97,6}, Y. Zhu⁶, S.C. Zugravel ⁵⁵, N. Zurlo ^{131,54}

Affiliation Notes

^I Deceased

^{II} Also at: Max-Planck-Institut für Physik, Munich, Germany

^{III} Also at: Italian National Agency for New Technologies, Energy and Sustainable Economic Development (ENEA), Bologna, Italy

^{IV} Also at: Dipartimento DET del Politecnico di Torino, Turin, Italy

^V Also at: Department of Applied Physics, Aligarh Muslim University, Aligarh, India

^{VI} Also at: Institute of Theoretical Physics, University of Wrocław, Poland

^{VII} Also at: An institution covered by a cooperation agreement with CERN

Collaboration Institutes

¹ A.I. Alikhanyan National Science Laboratory (Yerevan Physics Institute) Foundation, Yerevan, Armenia

² AGH University of Science and Technology, Cracow, Poland

³ Bogolyubov Institute for Theoretical Physics, National Academy of Sciences of Ukraine, Kiev, Ukraine

⁴ Bose Institute, Department of Physics and Centre for Astroparticle Physics and Space Science (CAPSS), Kolkata, India

⁵ California Polytechnic State University, San Luis Obispo, California, United States

⁶ Central China Normal University, Wuhan, China

⁷ Centro de Aplicaciones Tecnológicas y Desarrollo Nuclear (CEADEN), Havana, Cuba

⁸ Centro de Investigación y de Estudios Avanzados (CINVESTAV), Mexico City and Mérida, Mexico

⁹ Chicago State University, Chicago, Illinois, United States

¹⁰ China Institute of Atomic Energy, Beijing, China

¹¹ Chungbuk National University, Cheongju, Republic of Korea

¹² Comenius University Bratislava, Faculty of Mathematics, Physics and Informatics, Bratislava, Slovak Republic

¹³ COMSATS University Islamabad, Islamabad, Pakistan

¹⁴ Creighton University, Omaha, Nebraska, United States

¹⁵ Department of Physics, Aligarh Muslim University, Aligarh, India

¹⁶ Department of Physics, Pusan National University, Pusan, Republic of Korea

¹⁷ Department of Physics, Sejong University, Seoul, Republic of Korea

¹⁸ Department of Physics, University of California, Berkeley, California, United States

¹⁹ Department of Physics, University of Oslo, Oslo, Norway

²⁰ Department of Physics and Technology, University of Bergen, Bergen, Norway

²¹ Dipartimento di Fisica, Università di Pavia, Pavia, Italy

²² Dipartimento di Fisica dell'Università and Sezione INFN, Cagliari, Italy

²³ Dipartimento di Fisica dell'Università and Sezione INFN, Trieste, Italy

²⁴ Dipartimento di Fisica dell'Università and Sezione INFN, Turin, Italy

²⁵ Dipartimento di Fisica e Astronomia dell'Università and Sezione INFN, Bologna, Italy

²⁶ Dipartimento di Fisica e Astronomia dell'Università and Sezione INFN, Catania, Italy

²⁷ Dipartimento di Fisica e Astronomia dell'Università and Sezione INFN, Padova, Italy

²⁸ Dipartimento di Fisica 'E.R. Caianiello' dell'Università and Gruppo Collegato INFN, Salerno, Italy

²⁹ Dipartimento DISAT del Politecnico and Sezione INFN, Turin, Italy

³⁰ Dipartimento di Scienze MIFT, Università di Messina, Messina, Italy

³¹ Dipartimento Interateneo di Fisica 'M. Merlin' and Sezione INFN, Bari, Italy

³² European Organization for Nuclear Research (CERN), Geneva, Switzerland

³³ Faculty of Electrical Engineering, Mechanical Engineering and Naval Architecture, University of Split, Split, Croatia

³⁴ Faculty of Engineering and Science, Western Norway University of Applied Sciences, Bergen, Norway

³⁵ Faculty of Nuclear Sciences and Physical Engineering, Czech Technical University in Prague, Prague, Czech Republic

³⁶ Faculty of Physics, Sofia University, Sofia, Bulgaria

³⁷ Faculty of Science, P.J. Šafárik University, Košice, Slovak Republic

- ³⁸ Frankfurt Institute for Advanced Studies, Johann Wolfgang Goethe-Universität Frankfurt, Frankfurt, Germany
- ³⁹ Fudan University, Shanghai, China
- ⁴⁰ Gangneung-Wonju National University, Gangneung, Republic of Korea
- ⁴¹ Gauhati University, Department of Physics, Guwahati, India
- ⁴² Helmholtz-Institut für Strahlen- und Kernphysik, Rheinische Friedrich-Wilhelms-Universität Bonn, Bonn, Germany
- ⁴³ Helsinki Institute of Physics (HIP), Helsinki, Finland
- ⁴⁴ High Energy Physics Group, Universidad Autónoma de Puebla, Puebla, Mexico
- ⁴⁵ Horia Hulubei National Institute of Physics and Nuclear Engineering, Bucharest, Romania
- ⁴⁶ Indian Institute of Technology Bombay (IIT), Mumbai, India
- ⁴⁷ Indian Institute of Technology Indore, Indore, India
- ⁴⁸ INFN, Laboratori Nazionali di Frascati, Frascati, Italy
- ⁴⁹ INFN, Sezione di Bari, Bari, Italy
- ⁵⁰ INFN, Sezione di Bologna, Bologna, Italy
- ⁵¹ INFN, Sezione di Cagliari, Cagliari, Italy
- ⁵² INFN, Sezione di Catania, Catania, Italy
- ⁵³ INFN, Sezione di Padova, Padova, Italy
- ⁵⁴ INFN, Sezione di Pavia, Pavia, Italy
- ⁵⁵ INFN, Sezione di Torino, Turin, Italy
- ⁵⁶ INFN, Sezione di Trieste, Trieste, Italy
- ⁵⁷ Inha University, Incheon, Republic of Korea
- ⁵⁸ Institute for Gravitational and Subatomic Physics (GRASP), Utrecht University/Nikhef, Utrecht, Netherlands
- ⁵⁹ Institute of Experimental Physics, Slovak Academy of Sciences, Košice, Slovak Republic
- ⁶⁰ Institute of Physics, Homi Bhabha National Institute, Bhubaneswar, India
- ⁶¹ Institute of Physics of the Czech Academy of Sciences, Prague, Czech Republic
- ⁶² Institute of Space Science (ISS), Bucharest, Romania
- ⁶³ Institut für Kernphysik, Johann Wolfgang Goethe-Universität Frankfurt, Frankfurt, Germany
- ⁶⁴ Instituto de Ciencias Nucleares, Universidad Nacional Autónoma de México, Mexico City, Mexico
- ⁶⁵ Instituto de Física, Universidade Federal do Rio Grande do Sul (UFRGS), Porto Alegre, Brazil
- ⁶⁶ Instituto de Física, Universidad Nacional Autónoma de México, Mexico City, Mexico
- ⁶⁷ iThemba LABS, National Research Foundation, Somerset West, South Africa
- ⁶⁸ Jeonbuk National University, Jeonju, Republic of Korea
- ⁶⁹ Johann-Wolfgang-Goethe Universität Frankfurt Institut für Informatik, Fachbereich Informatik und Mathematik, Frankfurt, Germany
- ⁷⁰ Korea Institute of Science and Technology Information, Daejeon, Republic of Korea
- ⁷¹ KTO Karatay University, Konya, Turkey
- ⁷² Laboratoire de Physique des 2 Infinis, Irène Joliot-Curie, Orsay, France
- ⁷³ Laboratoire de Physique Subatomique et de Cosmologie, Université Grenoble-Alpes, CNRS-IN2P3, Grenoble, France
- ⁷⁴ Lawrence Berkeley National Laboratory, Berkeley, California, United States
- ⁷⁵ Lund University Department of Physics, Division of Particle Physics, Lund, Sweden
- ⁷⁶ Nagasaki Institute of Applied Science, Nagasaki, Japan
- ⁷⁷ Nara Women's University (NWU), Nara, Japan
- ⁷⁸ National and Kapodistrian University of Athens, School of Science, Department of Physics, Athens, Greece
- ⁷⁹ National Centre for Nuclear Research, Warsaw, Poland
- ⁸⁰ National Institute of Science Education and Research, Homi Bhabha National Institute, Jatni, India
- ⁸¹ National Nuclear Research Center, Baku, Azerbaijan
- ⁸² National Research and Innovation Agency - BRIN, Jakarta, Indonesia
- ⁸³ Niels Bohr Institute, University of Copenhagen, Copenhagen, Denmark
- ⁸⁴ Nikhef, National institute for subatomic physics, Amsterdam, Netherlands
- ⁸⁵ Nuclear Physics Group, STFC Daresbury Laboratory, Daresbury, United Kingdom
- ⁸⁶ Nuclear Physics Institute of the Czech Academy of Sciences, Husinec-Řež, Czech Republic
- ⁸⁷ Oak Ridge National Laboratory, Oak Ridge, Tennessee, United States
- ⁸⁸ Ohio State University, Columbus, Ohio, United States
- ⁸⁹ Physics department, Faculty of science, University of Zagreb, Zagreb, Croatia
- ⁹⁰ Physics Department, Panjab University, Chandigarh, India

- ⁹¹ Physics Department, University of Jammu, Jammu, India
- ⁹² Physics Program and International Institute for Sustainability with Knotted Chiral Meta Matter (SKCM2), Hiroshima University, Hiroshima, Japan
- ⁹³ Physikalisches Institut, Eberhard-Karls-Universität Tübingen, Tübingen, Germany
- ⁹⁴ Physikalisches Institut, Ruprecht-Karls-Universität Heidelberg, Heidelberg, Germany
- ⁹⁵ Physik Department, Technische Universität München, Munich, Germany
- ⁹⁶ Politecnico di Bari and Sezione INFN, Bari, Italy
- ⁹⁷ Research Division and ExtreMe Matter Institute EMMI, GSI Helmholtzzentrum für Schwerionenforschung GmbH, Darmstadt, Germany
- ⁹⁸ Saga University, Saga, Japan
- ⁹⁹ Saha Institute of Nuclear Physics, Homi Bhabha National Institute, Kolkata, India
- ¹⁰⁰ School of Physics and Astronomy, University of Birmingham, Birmingham, United Kingdom
- ¹⁰¹ Sección Física, Departamento de Ciencias, Pontificia Universidad Católica del Perú, Lima, Peru
- ¹⁰² Stefan Meyer Institut für Subatomare Physik (SMI), Vienna, Austria
- ¹⁰³ SUBATECH, IMT Atlantique, Nantes Université, CNRS-IN2P3, Nantes, France
- ¹⁰⁴ Sungkyunkwan University, Suwon City, Republic of Korea
- ¹⁰⁵ Suranaree University of Technology, Nakhon Ratchasima, Thailand
- ¹⁰⁶ Technical University of Košice, Košice, Slovak Republic
- ¹⁰⁷ The Henryk Niewodniczanski Institute of Nuclear Physics, Polish Academy of Sciences, Cracow, Poland
- ¹⁰⁸ The University of Texas at Austin, Austin, Texas, United States
- ¹⁰⁹ Universidad Autónoma de Sinaloa, Culiacán, Mexico
- ¹¹⁰ Universidade de São Paulo (USP), São Paulo, Brazil
- ¹¹¹ Universidade Estadual de Campinas (UNICAMP), Campinas, Brazil
- ¹¹² Universidade Federal do ABC, Santo Andre, Brazil
- ¹¹³ University of Cape Town, Cape Town, South Africa
- ¹¹⁴ University of Houston, Houston, Texas, United States
- ¹¹⁵ University of Jyväskylä, Jyväskylä, Finland
- ¹¹⁶ University of Kansas, Lawrence, Kansas, United States
- ¹¹⁷ University of Liverpool, Liverpool, United Kingdom
- ¹¹⁸ University of Science and Technology of China, Hefei, China
- ¹¹⁹ University of South-Eastern Norway, Kongsberg, Norway
- ¹²⁰ University of Tennessee, Knoxville, Tennessee, United States
- ¹²¹ University of the Witwatersrand, Johannesburg, South Africa
- ¹²² University of Tokyo, Tokyo, Japan
- ¹²³ University of Tsukuba, Tsukuba, Japan
- ¹²⁴ University Politehnica of Bucharest, Bucharest, Romania
- ¹²⁵ Université Clermont Auvergne, CNRS/IN2P3, LPC, Clermont-Ferrand, France
- ¹²⁶ Université de Lyon, CNRS/IN2P3, Institut de Physique des 2 Infinis de Lyon, Lyon, France
- ¹²⁷ Université de Strasbourg, CNRS, IPHC UMR 7178, F-67000 Strasbourg, France, Strasbourg, France
- ¹²⁸ Université Paris-Saclay Centre d'Etudes de Saclay (CEA), IRFU, Département de Physique Nucléaire (DPhN), Saclay, France
- ¹²⁹ Università degli Studi di Foggia, Foggia, Italy
- ¹³⁰ Università del Piemonte Orientale, Vercelli, Italy
- ¹³¹ Università di Brescia, Brescia, Italy
- ¹³² Variable Energy Cyclotron Centre, Homi Bhabha National Institute, Kolkata, India
- ¹³³ Warsaw University of Technology, Warsaw, Poland
- ¹³⁴ Wayne State University, Detroit, Michigan, United States
- ¹³⁵ Westfälische Wilhelms-Universität Münster, Institut für Kernphysik, Münster, Germany
- ¹³⁶ Wigner Research Centre for Physics, Budapest, Hungary
- ¹³⁷ Yale University, New Haven, Connecticut, United States
- ¹³⁸ Yonsei University, Seoul, Republic of Korea
- ¹³⁹ Zentrum für Technologie und Transfer (ZTT), Worms, Germany
- ¹⁴⁰ Affiliated with an institute covered by a cooperation agreement with CERN
- ¹⁴¹ Affiliated with an international laboratory covered by a cooperation agreement with CERN.